Comparative oncology reveals DNMT3B as a molecular vulnerability in undifferentiated pleomorphic sarcoma

Ashley M. Fuller[1,2,3,7,9], **Ann DeVine**[1,2,3,7,9], **Ileana Murazzi**[9], **Nicola J. Mason**[4,5,8,9], **Kristy Weber**[3,6,7,9], **T. S. Karin Eisinger-Mathason**[1,2,3,7,9,*]

[1]Abramson Family Cancer Research Institute

[2]Department of Pathology and Laboratory Medicine

[3]Penn Sarcoma Program

[4]Department of Clinical Sciences and Advanced Medicine

[5]Department of Pathobiology

[6]Department of Orthopaedic Surgery

[7]Perelman School of Medicine

[8]School of Veterinary Medicine

[9]University of Pennsylvania, Philadelphia, PA 19104 USA

Abstract

Purpose—Undifferentiated pleomorphic sarcoma (UPS), an aggressive subtype of soft-tissue sarcoma (STS), is exceedingly rare in humans and lacks effective, well-tolerated therapies. In contrast, STS are relatively common in canine companion animals. Thus, incorporation of veterinary patients into studies of UPS offers an exciting opportunity to develop novel therapeutic strategies for this rare human disease. Genome-wide studies have demonstrated that UPS is characterized by aberrant patterns of DNA methylation. However, the mechanisms and impact of this epigenetic modification on UPS biology and clinical behavior are poorly understood.

Methods—DNA methylation in mammalian cells is catalyzed by the canonical DNA methyltransferases DNMT1, DNMT3A and DNMT3B. Therefore, we leveraged cell lines and tissue specimens from human and canine patients, together with an orthotopic murine model, to probe the functional and clinical significance of DNMTs in UPS.

Results—We found that the DNA methyltransferase DNMT3B is overexpressed in UPS relative to normal mesenchymal tissues and is associated with a poor prognosis. Consistent with these findings, genetic DNMT3B depletion strongly inhibited UPS cell proliferation and tumor progression. However, existing hypomethylating agents, including the clinically approved drug 5-aza-2'-deoxycytidine and the DNMT3B-inhibiting tool compound nanaomycin A, were ineffective in UPS due to cellular uptake and toxicity issues.

Conclusions—DNMT3B represents a promising molecular susceptibility in UPS, but further development of DNMT3B-targeting strategies for these patients is required.

1   Introduction

Soft tissue sarcomas (STS) are heterogeneous tumors that arise in mesenchymal tissues such as muscle, adipose and fibrous connective tissue. Although STS account for only ~1% of all adult cancer cases, more than 70 histologic subtypes have been identified that differ on the basis of their tissue of origin, molecular features and clinical behavior [1]. Despite this heterogeneity, the majority of adult STS are karyotypically complex and exhibit a diverse spectrum of mutations and chromosomal abnormalities. As a result, these tumors are typically refractory to treatment with currently available targeted therapies, leaving patients with few options beyond surgical resection or amputation, radiation and/or chemotherapy [2]. Undifferentiated pleomorphic sarcoma (UPS), which predominantly arises in adult skeletal muscle, is a relatively common and particularly aggressive karyotypically complex subtype with a 10-year survival rate of only ~25% [3, 4]. Thus, development of more effective and better-tolerated treatment strategies for this disease represents an unmet clinical need.

DNA methylation of tumor suppressor gene promoters and the transcriptional silencing that ensues is a well-established feature of many cancers, including UPS [5–13]. More recent studies have also shown that gene body methylation, which is associated with transcriptional upregulation, is an important characteristic of tumor epigenetic landscapes that correlates with increased oncogene dosage [14, 15]. In STS, the majority of studies pertaining to aberrant DNA methylation patterns have done little to address the mechanistic basis and functional consequences thereof, focusing instead on improving tumor classification/diagnosis and patient risk stratification [5–11, 13]. Therefore, further functional studies in this area, particularly *in vivo*, are necessary. In mammalian cells, DNA methylation is catalyzed by the canonical DNA methyltransferases DNMT1, DNMT3A and DNMT3B [16]. Thus, these proteins are attractive candidates for enabling a better understanding of the mechanisms and impact of aberrant DNA methylation on UPS biology.

Comparative oncology integrates spontaneous cancers in animals, most notably canine companion animals, into studies of human tumor biology and therapy [17]. In contrast to some murine models of cancer, tumors in pet dogs develop in exclusively immunocompetent settings, exhibit cancer cell-intrinsic and microenvironmental heterogeneity, and can display similar therapeutic responses as their human counterparts [17–19]. Although some highly prevalent human cancers, such as breast, prostate and lung carcinomas, are rare in dogs [18], STS are relatively common, comprising ~15% of canine malignancies [20]. Moreover, although canine STS are not routinely subjected to detailed subtype classification, several studies have demonstrated that the histologic features of canine sarcomas parallel those of many human subtypes, including UPS [21–25]. Therefore, canine "models" of STS offer a unique opportunity to advance our understanding of and develop novel therapeutic strategies for this rare human cancer.

Herein, we adopt a comparative oncology approach to probe the functional and clinical significance of canonical DNMTs in UPS. Using cell lines and tissue specimens obtained from both human and canine patients, we show that DNMT3B overexpression is associated with poor clinical outcomes in UPS, and that functional depletion of this enzyme potently arrests UPS growth both *in vitro* and *in vivo*. We also show that an existing clinically approved DNA hypomethylating agent, 5-aza-2'-deoxycytidine, is an ineffective therapeutic strategy for human and canine UPS patients due to the limited ability of this compound to enter UPS cells/tissues. Similarly, a putative DNMT3B inhibitor, nanaomycin A, manifested *in vivo* toxicity in murine models. Nevertheless, taken together, our data indicate that development of DNMT3B-specific inhibitors for UPS patients is a promising avenue for future research.

2 Materials and methods

2.1 Cells and culture conditions

HEK293T, HT-1080 and C2C12 cells were purchased from the American Type Culture Collection (ATCC, Manassas, VA, USA). Human (HSMMs) and canine (CnSkMCs) skeletal muscle myoblasts were purchased from Lonza (Walkersville, MD, USA) and Cell Applications, Inc. (San Diego, CA, USA), respectively. KP230 cells were derived from murine *LSL-Kras*$^{G12D/+}$; *Trp53*$^{fl/fl}$ UPS tumors as described in [26]. STS-109 and STS-148 cells were derived from *TP53*-null UPS patient tumors and were a gift from Rebecca Gladdy, MD (University of Toronto, Canada). STSA-1 canine soft-tissue sarcoma cells were a gift from Molly Church, DVM, PhD (University of Pennsylvania School of Veterinary Medicine, Philadelphia, PA, USA). Upon receipt of each cell line, multiple aliquots were frozen in liquid nitrogen within 10 days of initial resuscitation. For experimental use, aliquots were thawed and cultured for up to 20 passages (4–6 weeks) before being discarded. HEK293T, HT-1080 and KP230 cells were cultured in DMEM with 10% FBS, 1% L-glutamine and 1% penicillin/streptomycin (P/S). STSA-1 cells were grown in DMEM with 15% FBS and 1% P/S. STS-109 and STS-148 cells were cultured in DMEM with 20% FBS, 1% L-glutamine and 1% P/S. C2C12 cells were grown in DMEM with 20% FBS and 1% P/S. HSMMs and CnSkMCs were cultured in SkGM-2 (CC-3245, Lonza) and CnSkMC (Cn151–500, Cell Applications, Inc.) growth medium, respectively. Sarcoma cell

lines were not permitted to exceed 50% confluence during routine culture or experiments, a standard approach in our laboratory. Myoblast cell lines C2C12, CnSkMC and HSMM were sub-cultured at 30–40% confluence. All cells were maintained in a humidified incubator at 37°C with 5% CO_2 and confirmed to be negative for mycoplasma contamination at the beginning of the study.

2.2 Oncomine and TCGA data analysis

The publicly available Detwiller et al. sarcoma dataset was used to analyze *DNMT3A* and *DNMT3B* expression levels in human UPS/FS and normal muscle specimens (access provided via Oncomine Research Premium Edition software, v4.5). For analysis of associations between *DNMT1*, *DNMT3A* and *DNMT3B* gene expression and human UPS patient survival, the TCGA-SARC dataset was downloaded from the NIH Genomic Data Commons portal, imported into and normalized with *DESeq2* [27] in R, and annotated with Ensembl BioMart. Clinical TCGA-SARC data ("TCGA, Cell 2017" dataset) were downloaded from cBioPortal on March 21, 2019; only cases included in the TCGA-SARC publication [10] were used in our analysis. Kaplan-Meier analyses were performed for disease-free, disease-specific and overall patient survival.

2.3 Lentiviral production and transduction

For shRNA-mediated knockdown studies, glycerol stocks of RNAi consortium lentiviral vectors were purchased from Dharmacon (Lafayette, CO, USA). A non-targeting scrambled control shRNA vector (sh:SCR) was purchased from Addgene (Watertown, MA, USA). Plasmids were packaged with the third-generation lentiviral packaging system (VSV-G, pMDLg, and pRSV-REV) and expressed in HEK293T cells via transient transfection with FuGENE 6 (Promega, Madison, WI, USA). Virus-containing supernatants were harvested after 24 and 48 hours, passed through 0.45 μm filters, mixed with PEG-8000 (Sigma-Aldrich, St. Louis, MO) at a 3:1 v/v ratio, and incubated overnight at 4°C. Supernatants were then centrifuged at $1500 \times g$ for 30 minutes at 4°C after which the virus-containing pellets were concentrated 80-fold in PBS. Aliquots were stored at −80°C and freeze-thawed a maximum of three times. For infection of sarcoma cell lines, cells were incubated overnight with lentiviral particles in the presence of 8.0 μg/ml polybrene (Sigma-Aldrich). Puromycin selection (3.0 μg/ml) was performed 48 hours after transduction and cells were harvested for analysis or used in further experiments after an additional 48 hours. Lentiviral constructs that exhibited the greatest knockdown efficiency in pilot analyses were used for all experiments: mouse *Dnmt3a*: TRCN0000039034 (sh:*Dnmt3a* #1) and TRCN0000039036 (sh:*Dnmt3a* #2); mouse *Dnmt3b*: TRCN0000071069 (sh:*Dnmt3b* #1) and TRCN0000071072 (sh:*Dnmt3b* #2); human *DNMT3A*: TRCN0000035755 (sh:*DNMT3A* #1) and TRCN0000035757 (sh:*DNMT3A* #2); human *DNMT3B*: TRCN0000035685 (sh:*DNMT3B* #1) and TRCN0000035686 (sh:*DNMT3B* #2); human *SLC29A1*: TRCN0000043645 (sh:*SLC29A1* #1) and TRCN0000043647 (sh:*SLC29A1* #2); human *SLC29A2*: TRCN0000043659 (sh:*SLC29A2* #1) and TRCN0000043660 (sh:*SLC29A2* #2). sh:*DNMT3B* #1 was not used in HT-1080 cells due to evidence of off-target effects (reduced proliferation without concomitant reductions in *DNMT3B* gene expression). To identify suitable shRNAs for use in canine sarcoma cells, all available mouse and human constructs were aligned to the canine *DNMT3A* or *DNMT3B* transcript (variant

1), as appropriate, using Standard Protein Blast (blastp). Acceptable shRNAs were defined as those that 1) possessed 100% query coverage in and 100% identity to the corresponding canine transcript, and 2) did not exhibit potential for off-target effects (defined as 100% query coverage in and 100% identity to a canine transcript other than the intended target). Based upon these criteria, human sh:*DNMT3B* #1 was the only shRNA suitable for use in canine cells (Supplementary Table 1). We were, however, unable to achieve consistent knockdown with this construct as assessed by qRT-PCR.

2.4 Cell proliferation (growth curve) assays

For shRNA studies, cells were transduced with lentiviral particles as described above, trypsinized 96 hours post-infection, and seeded at equal densities in puromycin-containing culture medium for the generation of growth curves. Cells were then counted using a hemocytometer with trypan blue exclusion every 2 days for 8 days (day 6, 8, 10 and 12 post-infection; STS-109 and STS-148 cells), or daily for 3 days (day 7, 8 and 9 post-infection; KP230, STSA-1 and HT-1080 cells). For siRNA studies, KP230 and HT-1080 cells were transfected with 50 nM mouse *Dnmt1* or human *DNMT1* ON-TARGETplus SMARTpool siRNAs with DharmaFECT reagent (Dharmacon) according to the manufacturer's instructions. Cells were then counted every 24 hours for 3 days.

For drug treatment (5-aza-2'-deoxycytidine; Sigma-Aldrich) studies with shRNAs, lentivirally infected HT-1080 cells were trypsinized 96 hours post-infection and seeded at equal densities in puromycin-containing culture medium. Cells were allowed to recover for 48 hours, after which they were treated with 50 nM DAC or vehicle control daily for 3 days. Cells were enumerated on day 9 post-infection. For drug treatment (nanaomycin A; Apex BioTechnology, Houston, TX, USA) studies without the use of shRNAs, cells were treated daily with nanaomycin A for 3 days with enumeration every 24 hours (KP230, STSA-1 and HT-1080 cells), or for 8 days with enumeration every 48 hours (STS-109 and STS-148 cells). To prepare DAC and nanaomycin A for *in vitro* use, each drug was diluted in DMSO to a final concentration of 1×10^7 nM after which single use aliquots were prepared and stored at $-80°C$. All drug treatments were administered in fresh culture medium. Specific concentrations used for each cell line are indicated in the text.

2.5 Orthotopic murine tumor model

Animal studies were performed in accordance with NIH guidelines and were approved by the University of Pennsylvania School of Medicine Animal Care and Use Committee. For *in vivo* knockdown studies, 6-week-old female nu/nu mice (strain code: 002019, The Jackson Laboratory, Bar Harbor, ME, USA) were randomized to receive bilateral orthoptic injections (into the gastrocnemius muscles) of 1×10^5 KP230 cells expressing a scrambled control, *Dnmt3a*- (sh:*Dnmt3a* #1) or *Dnmt3b*- (sh:*Dnmt3b* #2) targeting shRNA lentivirus. Each mouse received bilateral injections of the same cell type to reduce animal use (n = 5 mice or 10 tumors/group). Tumors were measured with electronic calipers every 24–48 hours and tumor volumes were calculated using the formula $(ab^2)\pi/6$ where "a" and "b" represent the longest and shortest dimensions, respectively. Animals were euthanized when the first tumor on each mouse reached the maximum allowed volume (1500 mm^3).

For *in vivo* nanaomycin A treatment, 6-week-old female nu/nu mice (The Jackson Laboratory) received unilateral orthotopic injections of 1×10^5 KP230 cells into the gastrocnemius muscle and were randomized to one of three groups: 0 mg/kg, 7.5 mg/kg or 15 mg/kg nanaomycin A (n = 10 mice/group). Nanaomycin A treatment for each mouse began when its respective tumor became palpable, and the drug was administered intraperitoneally (i.p.; 100 μl injection volume) every 48 hours for up to 3 weeks or until tumors reached the maximum allowed volume (1500 mm^3). Tumor volumes were measured and calculated as described above, and animal body weights were tracked to assess the impact of nanaomycin A treatment on overall health. To prepare nanaomycin A for *in vivo* delivery, the compound was reconstituted in DMSO to a final concentration of 5×10^7 nM, and single-use aliquots were made by dissolving the appropriate volume of drug in an aqueous solution of 45% PEG-400 (Sigma-Aldrich). In each 100 μl injection, the final concentration of DMSO was 30% (v/v) for all groups. Aliquots were stored at −80°C until use.

2.6 qRT-PCR assay

Total RNA was isolated from cells using the RNeasy Mini Kit (Qiagen, Germantown, MD, USA) and from tissue (~50–100 mg cut over dry ice) using TRIzol reagent (Thermo Fisher Scientific, Waltham, MA, USA). Reverse transcription of mRNA (up to 2 μg/reaction) was performed using the Applied Biosystems High-Capacity RNA-to-cDNA kit (Thermo Fisher Scientific). qRT-PCR (20 ng cDNA/reaction) was performed using TaqMan probes (Thermo Fisher Scientific) on an Applied Biosystems ViiA7 instrument. All TaqMan probes were "best coverage" assays except for canine *DNMT3B*, which was generated using the TaqMan custom design tool (Custom Plus TaqMan RNA assay ID ARAADW9). Hypoxanthine phosphoribosyltransferase, succinate dehydrogenase subunit A, and/or beta-2 microglobulin were used as endogenous controls.

2.7 RNA-sequencing and bioinformatics

Human STS-109 cells were transduced with *DNMT3A*- or *DNMT3B*-targeting shRNA lentiviruses (2 independent shRNAs per target) or a non-targeting shRNA control as described above, and lysed for total RNA isolation 96 hours after infection. RNA was extracted using the RNeasy Mini Kit with on-column DNase (Qiagen) and further purified with the RNA Clean and Concentrator Kit (Zymo Research, Irvine, CA, USA). Samples were quality-checked using the Agilent RNA 6000 Nano Kit and Agilent 2100 BioAnalyzer (Santa Clara, CA, USA). All samples had RNA integrity values of > 8.5. Poly(A) mRNA enrichment and library preparation were performed using the NEBNext Poly(A) mRNA Magnetic Isolation Module, NEBNext Ultra II RNA Library Prep Kit (New England BioLabs, Ipswitch, MA, USA) with SPRIselect Beads (Beckman Coulter, Brea, CA, USA), and NEBNext Multiplex Oligos for Illumina (index primers sets 1 and 2) according to the manufacturer's instructions. Library sizes were checked using the Agilent DNA 1000 Kit, and library concentrations were determined with Qubit dsDNA assays (Thermo Fisher Scientific). Equimolar amounts of each library were pooled, and pools were diluted to a final concentration of 1.8 pM in HT1 Hybridization Buffer (Illumina, San Diego, CA, USA) and sequenced on an Illumina NextSeq 500 instrument using the NextSeq 500/550 75-cycle High-Output Kit v2.5.

Illumina .bcl files were converted to FASTQ files using the Illumina *bcl2fastq* command line program. Salmon [28] was used to count raw expression data against the human transcriptome as defined in Gencode v32. Transcript-level data normalization and differential expression analysis (sh:*DNMT3A* vs. sh:SCR; sh:*DNMT3B* vs. sh:SCR) were performed with *DESeq2* [27]. To identify pathways that were differentially upregulated in sh:*DNMT3A* or sh:*DNMT3B* vs. control cells, we identified genes that were significantly upregulated (FDR-adjusted $p < 0.05$) in both shRNA comparisons for each target (i.e., genes upregulated in sh:*DNMT3A* #1 vs. sh:SCR and sh:*DNMT3A* #2 vs. sh:SCR). A similar process was carried out to identify genes that were significantly downregulated in both shRNA comparisons (i.e., genes downregulated in sh:*DNMT3A* #1 vs. sh:SCR and sh:*DNMT3A* #2 vs. sh:SCR). Additionally, to identify genes that were regulated by both *DNMT3A* and *DNMT3B*, we identified genes that were either up- or down-regulated in all 4 possible comparisons (i.e., genes significantly upregulated in sh:*DNMT3A* #1 vs. sh:SCR, sh:*DNMT3A* #2 vs. sh:SCR, sh:*DNMT3B* #1 vs. sh:SCR, and sh:*DNMT3B* #2 vs. sh:SCR). Pathway analyses on these "merged" gene lists were performed with Metascape [29].

2.8 Immunoblotting assay

Cells were lysed in 1x RIPA buffer supplemented with 1x protease and phosphatase inhibitors, after which lysate concentrations were determined using the Pierce BCA Protein Assay Kit (Thermo Fisher Scientific). Denatured proteins were separated by electrophoresis on sodium dodecyl sulfate-polyacrylamide gels, transferred to 0.2 μm PVDF membranes using the Bio-Rad Trans-Blot Turbo System (Hercules, CA, USA), blocked for 30–60 minutes in 5% non-fat dry milk, and probed with the following antibodies overnight at 4°C: rabbit anti-DNMT3A (0.2 μg/ml [1:500]; HPA026588, Atlas Antibodies, Stockholm, Sweden), rabbit anti-DNMT3B (0.4 μg/ml [1:500]; HPA001595, Atlas Antibodies), rabbit anti-Dnmt3b (0.5–1.0 μg/ml [1:1:000–1:2000]; NB300–516, Novus Biologicals, Centennial, CO, USA), rabbit anti-cyclin D1 (1:2000; 26939–1-AP, Proteintech, Rosemont, IL, USA), rabbit anti-cyclin A2 (1:5000 [KP230 and STS-109 cells] or 1:10000 [HT-1080 cells]; 18202–1-AP, Proteintech), mouse anti-ENT1 (2 μg/ml [1:100]; F12 sc-377283, Santa Cruz Biotechnology, Dallas, TX, USA), mouse anti-ENT2 (2 μg/ml [1:100]; D9 sc-373871, Santa Cruz Biotechnology), rabbit anti-b-actin (1:10000; #8227, Abcam, Waltham, MA, USA), and rabbit anti-GAPDH (1:2500–1:5000; #2118, Cell Signaling Technology, Danvers, MA, USA). Next, membranes were probed with horseradish peroxidase-conjugated anti-rabbit or anti-mouse secondary antibodies (1:2500; #7074 and #7076, Cell Signaling Technology) for 1 hour at room temperature. Chemiluminescent detection was performed with Western Lightning Plus-ECL reagent (PerkinElmer, Waltham, MA, USA).

2.9 Immunohistochemistry and digital histopathology

Human sarcoma tissue microarrays (TMAs) were purchased from US Biomax, Inc. (SO801a, Derwood, MA, USA). Murine tumors were formalin-fixed, paraffin-embedded, sectioned at 5 μm, and stained with hematoxylin and eosin (H&E) according to standard protocols. Tumor histomorphology was reviewed by a research fellow with formal training in histopathology (AMF). Immunohistochemistry was performed on a Bond RXm autostainer instrument with the Bond Polymer Refine Detection kit (Leica Biosystems, Buffalo Grove, IL, USA) using the following antibodies and epitope retrieval (ER) buffers:

rabbit anti-DNMT3A (2 μg/ml [1:50], 30 minutes with ER1; HPA026588, Atlas Antibodies), rabbit anti-DNMT3B (0.4 μg/ml [1:500], 30 minutes with ER1; HPA001595, Atlas Antibodies), and rabbit anti-p62 (1:2000, 30 minutes with ER1; PM045, MBL International, Woburn, MA, USA). Slides were scanned into digital images at a magnification of 20x using the Aperio VERSA 200 platform (Leica Biosystems). Images were annotated to exclude areas with poor resolution or that contained histologically normal cancer-adjacent tissue, folded tissue, debris or staining/scanning artifacts. Analyses were performed with Aperio ImageScope software (Leica Biosystems) as follows: To assess nuclear DNMT3A and DNMT3B staining in tumor tissue, the "nuclear V9" algorithm was tuned to UPS cores from the human sarcoma TMA. To assess nuclear DNMT3A and DNMT3B staining in normal skeletal muscle tissue, skeletal muscle cores from the human sarcoma TMA were subjected to tissue composition analysis with the Aperio Genie Classifier. Use of this classifier was necessary to prevent detection/quantification of non-specific hematoxylin staining that was present in normal skeletal muscle cores but not in UPS cores. To train the composition estimator, normal skeletal muscle slides from an in-house tissue repository were randomly selected and manually annotated for skeletal muscle nuclear area, "other" tissue area, and glass. Following partitioning of each component, the same "nuclear V9" algorithms developed for assessment of DNMT3A and DNMT3B IHC staining in UPS cores were then applied to the "skeletal muscle nuclei" class of the normal skeletal muscle cores. Finally, the "positive pixel count" algorithm was used to quantify p62 staining in murine tumor tissues. A p62 IHC score was calculated as follows: ($3 \times$ % strong positive pixels) + ($2 \times$ % moderately positive pixels) + ($1 \times$ % weak positive pixels).

2.10   TUNEL assay and immunofluorescence analysis

Murine tumor sections were deparaffinized and rehydrated according to standard protocols and microwave-irradiated with 10 mM sodium citrate buffer, pH 6.0, for 10 minutes. Detection of DNA fragmentation was performed using the *In Situ* Cell Death Detection Kit, Fluorescein (Roche, Indianapolis, IN, USA) according to the manufacturer's instructions. Hoechst 33342 (1 μg/ml) was used as a nuclear counterstain and coverslips were mounted with ProLong Diamond Antifade Mountant (Thermo Fisher Scientific). Images (5 fields per tumor section) were acquired with a Nikon Eclipse Ni microscope and Nikon NES Elements software with pixel saturation monitoring. Areas with high levels of autofluorescence were avoided. Analysis of nuclear TUNEL staining was performed with Fiji as follows: Watershed analysis of DAPI channel images (8-bit) was performed to "separate" nuclei that appeared to be touching. Nuclei were then converted to regions of interest (ROIs) that were "applied" to the corresponding TUNEL/fluorescein channel image (8-bit format). The staining intensity in these nuclear ROIs was then calculated by normalizing the integrated density of TUNEL staining to the number of nuclei.

2.11   Cell cycle analysis and flow cytometry

KP230, STSA-1 and HT-1080 cells were transduced with lentiviral particles as described above or treated with nanaomycin A every 24 hours for 3 days; specific concentrations are noted in the text. Next, the cells were pulsed-labelled with 10 μM EdU (Click-iT EdU Alexa Fluor 488 Flow Cytometry Assay Kit, Thermo Fisher Scientific) in fresh culture medium for 1 hour, harvested via trypsinization, and fixed in ice-cold ethanol for at least 2 hours.

Detection of DNA synthesis was performed according to the manufacturer's instructions, after which cells were stained with 1 μg/ml Hoechst 33342 at a concentration of 1×10^6 cells/ml for evaluation of DNA content. Flow cytometric data were collected on an LSR II instrument with FACSDiva software (BD Biosciences, Franklin Lakes, NJ, USA). The instrument was run on the lowest flow-rate setting (~200 events/second) and at least 20,000 singlet events were captured for each sample. Analysis of cell cycle distribution was performed with FlowJo software (BD Biosciences) in which compensation and gating were guided by single-color controls (equivalent to fluorescence-minus-one controls in this experiment). For all cell lines, sub-G1 cells were gated out because events in this region may represent cell fragments rather than whole cells [30]. Additionally, for STSA-1 cells, G2/M-phase and polyploid cells were also gated out due to 1) the inability of our protocol to distinguish diploid G2/M cells from tetraploid G1 cells and 2) the highly variable proportion of polyploid cells in replicate experiments at baseline.

2.12 Myoblast differentiation studies

To induce myoblast differentiation, C2C12, CnSkMC and HSMM cells on gelatin-coated plates (Gelatin-based coating solution, Cell Biologics Inc., Chicago, IL, USA) were allowed to recover overnight in growth medium, after which they were switched to their respective differentiation medium (C2C12: sodium pyruvate-free DMEM + 2% horse serum + 1% P/S; CnSkMC: Canine Skeletal Muscle Differentiation Medium, Cell Applications, Inc.; HSMM: DMEM/F12 with 15 mM HEPES + 2% horse serum + 1% P/S) for 6 days (C2C12) or 5 days (CnSkMC and HSMM).The cells were plated such that they would reach ~80–90% confluence by the end of the differentiation period (C2C12: ~2.1×10^4 cells/cm^2; CnSkMC: ~1.0×10^4 cells/cm^2; HSMM: ~1.0×10^4 cells/cm^2). In addition, proliferating cells grown overnight to ~40–50% confluence (C2C12: ~7800 cells/cm^2; CnSkMC: ~2.1×10^4 cells/cm^2; HSMM: ~1.0×10^4 cells/cm^2) were used in each experiment to confirm successful induction of differentiation (qRT-PCR-based analysis of species-specific skeletal muscle differentiation markers).

To assess the impact of nanaomycin A on myoblast viability, myoblasts were differentiated as described above in the absence of nanaomycin A, and subsequently treated with nanaomycin A every 24 hours for 3 days. Percent viability was determined every 24 hours using a hemocytometer with trypan blue exclusion. Accutase was used to dissociate differentiated HSMMs because it was less toxic to these cells than trypsin. To assess the impact of nanaomycin A on myoblast differentiation to myotubes, cells were differentiated as described above in the presence or absence of nanaomycin A (daily treatments; specific concentrations used for each cell line are indicated in the text). HSMM cells, which underwent nanaomycin A treatment withdrawal, were maintained in nanaomycin A-free differentiation medium for an additional 5 days after the final drug treatment. For all experiments, nanaomycin A was diluted in DMSO and treatments were administered in fresh culture medium.

3 Results

3.1 UPS response heterogeneity to the clinical DNA methylation inhibitor 5-aza-2'-deoxycytine (DAC): role of solute carrier 29 (*SLC29*) family expression

In clinical oncology settings, inhibition of DNA methylation is achieved with cytidine analogs such as 5-aza-2'-deoxycytidine (Decitabine; DAC). This compound incorporates into DNA and impedes cell proliferation by enabling DNA demethylation and re-expression of previously silenced genes (e.g., cell cycle regulators; pro-apoptotic genes), or by forming irreversible covalent adducts with DNMTs and inducing DNA damage [31, 32]. DAC is FDA-approved for patients with myelodysplastic syndrome and has been studied extensively in *in vitro*, pre-clinical and clinical studies of hematologic cancers and carcinomas (PubChem: CID 451668, Decitabine; clinicaltrials.gov). However, the therapeutic efficacy of DAC in sarcoma remains underexplored. To address this knowledge gap, we treated two human patient-derived UPS cell lines with clinically relevant nanomolar doses [33] of DAC and assessed its impact on cell proliferation. We also included HT-1080 fibrosarcoma (FS) cells in this analysis because certain FS subtypes, such as myxofibrosarcoma (MFS), are now thought to be genetically indistinguishable from UPS [10]. We found that DAC significantly reduced the proliferation of HT-1080 and STS-109 cells at one or more time points in a dose-dependent manner ("strong responders") with little impact on cell viability (Fig. 1a). In contrast, STS-148 cells responded weakly to DAC, with statistically significant, yet biologically modest, reductions in proliferation only apparent after exposure to the highest dose for the longest treatment interval (Fig. 1a). DAC is taken up into cells via the equilibrative nucleoside transporters hENT1 and hENT2 (encoded by *SLC29A1* and *SLC29A2*, respectively), and *SLC29A1* expression levels have been found to inversely correlate with DAC IC_{50} values in human carcinoma and hematologic cancer cell lines [34]. Therefore, we reasoned that differences in *SLC29A1* and/or *SLC29A2* gene expression may underlie the DAC response heterogeneity observed among human UPS and FS cells. Consistent with this hypothesis, the strong responders (HT-1080 and STS-109) exhibited significantly higher expression levels of one or both nucleoside transporters than the weakly responding STS-148 cells (Fig. 1b). At the protein level, similar trends in hENT1 expression were observed, whereas hENT2 expression tracked less closely with transcriptional patterns (Fig. 1c). Thus, DAC responsivity in human UPS/FS cell lines correlates with the expression of *SLC29A1*/hENT1, and to a lesser extent with that of *SLC29A2*/hENT2.

To determine whether hENT1 and/or hENT2 are required for UPS/FS cell DAC susceptibility, we transduced HT-1080 cells (a strong responder) with shRNAs targeting *SLC29A1* or *SLC29A2*, and treated them with 50 nM DAC every 24 hours for 3 days (Fig. 1d). HT-1080 cells were used in this experiment because they are more easily transduced than primary UPS cells (STS-109). Whereas knocking down these transporter genes almost completely ceased cell proliferation in pilot studies, 1/10 the typical amount of lentivirus was used in this experiment to generate a sufficient number of cells for further analysis. Reductions in cell growth were also observed with this modified infection protocol, but cells were still able to proliferate, albeit slowly, during the experiment (Fig. 1e). HT-1080 cells expressing a scrambled control shRNA (sh:SCR) exhibited a ~43% decrease in proliferation following DAC treatment (Fig. 1f). This DAC-induced proliferation deficit was significantly

attenuated after depletion of *SLC29A1*, but not *SLC29A2* (Fig. 1f). In all cases, DAC did not substantially impact cell viability. Furthermore, we were unable to assess the effects of dual *SLC29A1*/*SLC29A2* knockdown due to toxicity. Although the reduced baseline proliferation observed following *SLC29A1* or *SLC29A2* depletion may have confounded the results of this experiment, our results nevertheless indicate that *SLC29A1*/hENT1 expression is an important regulator of DAC susceptibility in UPS.

To determine the applicability of these relationships to human tissue, we examined *SLC29A1* and *SLC29A2* gene expression patterns in samples from two independent sarcoma patient cohorts: 1) the publicly available Detwiller et al. sarcoma dataset [35; Oncomine] and 2) samples procured through the University of Pennsylvania Surgical Pathology service ("UPenn cohort"). In both cohorts, *SLC29A2* expression was reduced in the majority of UPS/(M)FS specimens relative to normal skeletal muscle and connective tissue, whereas *SLC29A1* expression displayed greater intertumoral heterogeneity (Fig. 1g–h; Supplementary Table 2). We also ascertained the relevance of our findings to canine companion animals by leveraging sarcoma tissue specimens procured by the University of Pennsylvania School of Veterinary Medicine ("Penn Vet cohort") and canine STSA-1 grade II STS cells [36]. The tumor from which these cells were derived was not classified as a particular subtype but resembled UPS with respect to its skeletal muscle origin, pleomorphic histology, and invasive and metastatic behavior [36]. Data from canine cells and tissue largely recapitulated that from our human system: STSA-1 cell proliferation was resistant to clinically relevant doses of DAC (Fig. 1i), similar to human STS-148 cells. Moreover, *SLC29A2* was downregulated in the majority of canine STS specimens relative to normal skeletal muscle, while *SLC29A1* expression tended to be more variable (Fig. 1j). Taken together, our findings suggest that expression of these transporters – and *SLC29A1* in particular – in human UPS and canine sarcoma tissue is heterogeneous, as are cellular responses to DAC. Accordingly, we posit that this intertumoral heterogeneity will preclude the clinical efficacy of DAC in many human and canine UPS patients, illustrating a need for the development of novel DNA methylation inhibitors.

3.2 *DNMT3A* and *DNMT3B* regulate UPS cell proliferation *in vitro* and *in vivo*

We next sought to identify more specific and less heterogeneous targets for inhibition of DNA methylation in human UPS and canine sarcoma. We focused on the canonical DNMT proteins DNMT1, DNMT3A and DNMT3B, which catalyze DNA methylation in mammalian cells [16]. First, we performed cell-based proliferation assays to evaluate the functional role of these enzymes in this tumor context. In addition to our human and canine cell lines, we also used murine KP230 cells, derived from the $Kras^{G12D/+}$; $Trp53^{fl/fl}$ (KP) genetically engineered mouse model of UPS [26]. In this model, injection of adeno-Cre virus into the gastrocnemius muscle leads to the development of skeletal muscle tumors that molecularly and histologically recapitulate human UPS [37, 38]. Genetic depletion studies in mouse and human cells were performed with gene-specific siRNA pools or lentiviral shRNAs (2 independent shRNAs per target gene). These analyses were not performed in canine STSA-1 cells because rigorously validated canine siRNAs are not widely available, nor were we able to achieve consistent or specific gene silencing with our shRNA lentivirus system (see Methods; Supplementary Table 1). We observed no significant effects on

UPS cell growth after depletion of *Dnmt1*/*DNMT1* (Supplementary Fig. 1a–d). However, *Dnmt3a*/*DNMT3A* silencing significantly reduced the proliferation of KP230, STS-109, STS-148 and HT-1080 cells (Fig. 2a–d, Supplementary Fig. 1e–h), with similar results obtained for *Dnmt3b*/*DNMT3B* knockdown (Fig. 2e–h, Supplementary Fig. 1i–l). These data indicate that the KP model successfully recapitulates aspects of human UPS with respect to DNMT function. Furthermore, in some cases, *DNMT3A* or *DNMT3B* silencing reduced the number of viable human cells over time (relative to the starting number of cells), indicative of cell death (Fig. 2c, g; Supplementary Fig. 1i). However, this result was heterogeneous across human cell lines and not consistently observed with both shRNA constructs for each gene.

To determine the role of *Dnmt3a* and *Dnmt3b* in tumor progression, we injected 6-week-old nude mice orthotopically (into the gastrocnemius muscle) with 1×10^5 KP230 cells transduced with a scrambled control, *Dnmt3a*-, or *Dnmt3b*-targeting shRNA. Each mouse was injected bilaterally to reduce animal use and was euthanized when either intramuscular tumor reached the maximum allowed volume (1500 mm^3). Gene expression levels of *Dnmt3a* and *Dnmt3b* in KP230 cells immediately prior to orthotopic injection, as well as in bulk tumor tissue at the conclusion of the assay, are shown in Fig. 2i and Supplementary Fig. 1m, respectively. H&E staining revealed that *Dnmt3a* or *Dnmt3b* depletion did not appear to impact tumor morphology (Supplementary Fig. 1n). sh:*Dnmt3b* tumors were significantly smaller than control and/or sh:*Dnmt3a* tumors beginning on day 18 of the study (Fig. 2j), eventually reaching the maximum volume on day 33 (Supplementary Fig. 1o). sh:*Dnmt3a* tumors were also significantly smaller than control tumors, but reached the maximum volume more rapidly than sh:*Dnmt3b* tumors. Consistent with this observation, mice bearing sh:*Dnmt3b* tumors experienced significantly longer survival than animals bearing control ($p = 0.0017$) and sh:*Dnmt3a* ($p = 0.0042$) tumors (Fig. 2k). Animals with sh:*Dnmt3a* tumors also tended to experience prolonged survival compared to control mice, but this comparison did not reach statistical significance. Moreover, among the tumors that had not reached maximum volume at the time of euthanasia, including one sh:*Dnmt3b* tumor that never formed, *Dnmt3b*-deficient tumors were smaller than both control and *Dnmt3a*-deficient tumors (Supplementary Fig. 1p). Taken together, our results indicate that *Dnmt3a*/*DNMT3A* and *Dnmt3b*/*DNMT3B* both control UPS cell proliferation, but that depletion of *Dnmt3b* more effectively restrains tumor progression *in vivo*.

3.3 *Dnmt3b*/*DNMT3B* deficiency inhibits DNA synthesis in UPS cells

To understand more specifically how *DNMT3B* controls UPS cell proliferation, we performed RNA-seq on human STS-109 cells expressing a scrambled control or one of two independent *DNMT3B*-targeting shRNAs. Differential expression analysis was performed to identify genes that were significantly up- or downregulated (FDR $p < 0.05$) in response to both *DNMT3B*-targeting shRNAs compared to the control (Fig. 3a–b). Metascape analysis of the resulting gene lists indicated that pathways related to autophagy, apoptosis and protein metabolism were significantly upregulated in sh:*DNMT3B* cells compared to the control (Fig. 3a), whereas pathways pertaining to DNA replication and cell cycle progression were significantly downregulated (Fig. 3b). A similar analysis in STS-109 cells expressing *DNMT3A*-specific shRNAs revealed that pathways regulated by *DNMT3A* were distinct

from those regulated by *DNMT3B* (Supplementary Fig. 2a–b). In fact, only 87 genes were significantly upregulated in both sh:*DNMT3A* and sh:*DNMT3B* cells compared to the control, whereas only 65 genes were significantly downregulated (FDR $p < 0.05$; Supplementary Fig. 2c; Supplementary Table 3).

We used samples from our murine orthotopic tumor study to explore these potential mechanisms in more detail. No evidence of significantly increased apoptosis was found in sh:*Dnmt3b* vs. sh:SCR specimens (Supplementary Fig. 2d–e), nor did we observe significant differences in the expression of p62 (Supplementary Fig. 2f–h), an autophagic substrate that is degraded when autophagy is induced [39, 40]. Therefore, we considered the role of cell cycle regulation. In a qRT-PCR-based screen of cell cycle regulators, *Cdkn3*, a cyclin-dependent kinase inhibitor that opposes the G1-S transition [41], was upregulated by ~50% in sh:*Dnmt3b* compared to sh:SCR tumors ($p = 0.0526$; Fig. 3c). We therefore performed flow cytometry to obtain a more comprehensive understanding of cell cycle dynamics in *Dnmt3b*/*DNMT3B*-deficient cells (gating strategy provided in Supplementary Fig. 3a). In both mouse (KP230) and human (HT-1080) cells, *Dnmt3b*/*DNMT3B* silencing significantly reduced the proportion of cells in S-phase and concomitantly increased the proportion of cells in G1-phase (Fig. 3d–f). For all samples, we confirmed proper gate placement around G1- and G2/M-phase cells using the median fluorescence intensity (MFI) of Hoechst 33342-DNA staining in these populations (Supplementary Fig. 3b). All samples had a G2/G1 MFI ratio of ~2, confirming that the DNA content of G2/M-phase cells was twice that of G1-phase cells. To confirm these flow cytometric data, we performed Western blot analyses to query the expression of cyclin D1 and cyclin A2, G1- and S-phase cyclins, respectively, in *Dnmt3b*/*DNMT3B*-deficient and control cells. In murine KP230 cells, cyclin D1 was markedly reduced in the setting of *Dnmt3b* depletion (Fig. 3g), consistent with the induction of G1-phase arrest [42]. In contrast, cyclin A2 levels remained relatively stable (Fig. 3g). Conversely, *DNMT3B*-deficient human HT-1080 cells exhibited modestly reduced cyclin A2 levels, with no consistent changes in cyclin D1 expression (Fig. 3h). A second human cell line, STS-109, also displayed attenuated cyclin A2 levels in response to *DNMT3B* silencing (Fig. 3i). From these data we conclude that DNMT3B depletion impedes UPS/FS cell proliferation by inhibiting DNA synthesis, but that the precise cell cycle machinery impacted by this phenomenon differs between murine and human cells.

3.4 Nanaomycin A, a DNMT3B-inhibiting tool compound, potently inhibits UPS cell proliferation *in vitro*

Given the capacity of genetic *Dnmt3b*/*DNMT3B* depletion to restrain UPS growth both *in vitro* and *in vivo*, we sought a pharmacologic approach for clinical translation. Nanaomycin A, a quinone antibiotic, has been described as a DNMT3B-specific inhibitor with tumor-suppressive properties in human colon, lung and leukemia cell lines [43, 44]. Consistent with these reports, we found that nanaomycin A exhibited dose-dependent anti-proliferative activity in all five cell lines in our panel, with minimal cytotoxicity (Fig. 4a–c, Supplementary Fig. 4a–b, Supplementary Table 4). It was most potent in murine KP230 cells, which responded to as little as 10–50 nM after 2–3 days of exposure; no additional benefit was observed after treatment with 100 nM (Fig. 4a, Supplementary Table 4). Growth inhibition in canine and human cells was achieved with slightly higher concentrations (100–

500 nM; Fig. 4b–c, Supplementary Fig. 4a–b, Supplementary Table 4), but all doses used are considered clinically relevant according to commonly accepted preclinical drug screening conventions [45].

We next asked whether nanaomycin A suppresses cell proliferation via inhibition of DNA synthesis in a manner analogous to *DNMT3B* silencing (gating strategy for STSA-1 cells is shown in Supplementary Fig. 4c). Consistent with this hypothesis, nanaomycin A treatment significantly reduced the proportion of human HT-1080 cells in S-phase, increased the percentage of cells in G1-phase, and modestly reduced cyclin A2 expression levels without altering cyclin D1 expression (Fig. 4d–f, Supplementary Fig. 4d). Murine KP230 and canine STSA-1 cells displayed similar trends in cell cycle phase distributions, although the observed effects did not reach statistical significance (Supplementary Fig. 4e–g). Nevertheless, nanaomycin A-treated KP230 cells did exhibit attenuated cyclin A2 expression, indicative of reduced DNA synthesis (Supplementary Fig. 4h). However, unlike in response to *Dnmt3b* depletion (Fig. 3g), no alterations in cyclin D1 levels were observed in these cells (Supplementary Fig. 4h). These results may indicate the potential for off-target effects in murine UPS. Nevertheless, in human cells, our findings clearly demonstrate that nanaomycin A treatment phenocopies genetic *DNMT3B* deficiency, illustrating the potential clinical utility of this compound in human disease.

3.5 Evaluation of nanaomycin A toxicity in normal skeletal muscle cells and murine models

Due to the anti-neoplastic efficacy of nanaomycin A in cell-based models of UPS, we proceeded with *in vitro* functional and toxicity studies of untransformed skeletal muscle myoblasts, which are widely used *in vitro* models of normal skeletal muscle cells. First, we assessed whether nanaomycin A exposure impairs myoblast differentiation into multi-nucleated myotubes. We treated murine (C2C12), canine (CnSkMC) and human (HSMM) myoblasts with nanaomycin A daily during the course of differentiation, after which expression of skeletal muscle lineage markers [46–50] was measured by qRT-PCR (Supplementary Fig. 5a). Interestingly, we observed distinct species-specific responses. In C2C12 cells, nanaomycin A only minimally impacted differentiation, significantly reducing the expression of one gene, *Myh2*, by ~20% (Supplementary Fig. 5b). Conversely, in CnSkMC cells, nanaomycin A had inconsistent effects on gene expression at the lowest dose (100 nM), potentially due to mild toxicity, and was overtly cytotoxic at higher doses (50% and ~100% cell death at 250 and 500 nM, respectively; Supplementary Fig. 5c). Yet another distinct pattern was observed for HSMM cells, in that differentiation marker expression was reduced in a dose-dependent manner (Fig. 4g). Withdrawal of the drug for 5 days did not restore *MEF2C* gene expression, but did enable a partial recovery of *MYH2* expression (Fig. 4h). These data indicate that nanaomycin A impedes human myoblast differentiation, but that this effect is partially reversible when the drug is withdrawn.

In addition to testing the effects of nanaomycin A on myoblast differentiation, we also determined whether the compound was cytotoxic to differentiated myotubes. We found that nanaomycin A had inconsistent effects on the number of viable CnSkMC cells, reducing viability in a dose-dependent manner in some experimental replicates, but causing rapid,

uniform cell death in others (Supplementary Fig. 5d). However, it did not impact the viability of C2C12 or HSMM cells at any concentration (Supplementary Fig. 5d).

Encouraged by these findings, we evaluated the therapeutic potential of nanaomycin A *in vivo*. We injected 6-week-old nude mice orthotopically with 1×10^5 KP230 cells and administered nanaomycin A or vehicle control i.p. once tumors became palpable. Thereafter, animals were treated every 48 hours for three weeks or until tumors reached the maximum allowed volume (1500 mm^3; Supplementary Fig. 5e). Mice treated with 15 mg/kg nanaomycin A exhibited significantly longer survival than mice in the vehicle control group, with two animals in the 15 mg/kg group experiencing near-complete cessation of tumor growth (Fig. 4i–j). Unfortunately, however, these same two mice became cachectic and were humanely euthanized prior to the study endpoint. Similarly, body weights of the remaining mice in the 15 mg/kg group were significantly lower than those of control mice (Fig. 4k). In contrast, mice treated with 7.5 mg/kg nanaomycin A did not show signs of overt toxicity, but this dose did not significantly inhibit tumor progression or extend survival relative to the vehicle control (Fig. 4i–k). These findings indicate that nanaomycin A exhibits toxicity and limited efficacy *in vivo*, precluding its use in clinical settings. Nevertheless, our *in vitro* studies clearly indicate that DNMT3B appears to be a promising molecular vulnerability in UPS, warranting the development of novel inhibitors.

3.6 DNMT3B and DNMT3A are highly expressed in UPS and associated with a poor prognosis

To determine the extent to which continued development of pharmacologic DNMT3B inhibitors would have clinical utility, we characterized DNMT3B expression patterns in UPS and normal mesenchymal tissues. Given that DNMT3A depletion also showed anti-neoplastic activity *in vivo*, albeit to a lesser extent than that of DNMT3B, we also considered DNMT3A in this analysis in the event development of DNMT3B-specific inhibitors is ultimately not feasible due to unfavorable pharmacokinetic/pharmacodynamic profiles or toxicity concerns. Analysis of samples in the UPenn cohort and Detwiller sarcoma dataset revealed strong upregulation of *DNMT3B* gene expression in UPS/(M)FS samples relative to normal muscle and connective tissue (Fig. 5a–b). *DNMT3A* gene expression was generally more stable than that of *DNMT3B*, particularly in the UPenn cohort, but was increased in a subset of UPS/FS specimens in the Detwiller dataset (Fig. 5a–b). Similar trends were observed in canine samples from the Penn Vet cohort (Fig. 5c). We also performed immunohistochemistry (IHC) for DNMT3B and DNMT3A on human sarcoma TMAs containing UPS and normal skeletal muscle specimens (n = 11 and n = 5, respectively; Supplementary Fig. 6a; Supplementary Table 5). These samples exhibited prominent nuclear immunoreactivity with relatively scant cytoplasmic staining (Fig. 5d). Quantification of nuclear DNMT3B staining revealed significant upregulation in UPS compared to skeletal muscle tissue (Fig. 5e, Supplementary Fig. 6b). Interestingly, in contrast to our gene expression results, nuclear DNMT3A expression was also significantly increased in tumors relative to normal muscle, suggesting that DNMT3A levels are subject to post-transcriptional regulation in UPS cells (Fig. 5e, Supplementary Fig. 6b). Ultimately, more than 70% of nuclei in all tumors examined were positive for at least one DNMT3 isoform. Consistent with this observation, DNMT3B and DNMT3A nuclear

percent positivity were found to be moderately correlated in UPS tumors (Pearson r = 0.5001; Fig. 5f) according to conventional benchmarks for interpretation of correlation coefficients [51]. In contrast, nuclear DNMT3B and DNMT3A positivity in normal skeletal muscle were more heterogeneous but more strongly correlated (Pearson r = 0.9302; Fig. 5g).

Finally, we queried the Cancer Genome Atlas Sarcoma (TCGA-SARC) dataset to evaluate associations between the expression of DNMT-encoding genes and human UPS patient survival (n = 44). Consistent with our findings in UPS cell lines, expression of *DNMT1* was not associated with any survival endpoint (Supplementary Fig. 6c–e). However, high levels of *DNMT3B* and *DNMT3A* strongly tracked with reduced disease-specific (Fig. 5h–i), overall (Supplementary Fig. 6f–g) and disease-free survival (Supplementary Fig. 6h–i). Taken together, these findings indicate that DNMT3B and DNMT3A serve as critical factors in UPS patient survival, and that modulation of their activity and/or expression may improve clinical outcomes.

4   Discussion

Comparative oncology is a powerful, often underutilized approach for elucidating fundamental mechanisms of tumor biology and developing novel therapeutic strategies [20]. Due to the high prevalence of STS in pet dogs compared to human adults (~15% vs. ~1% of cases, respectively) [1, 20], canine companion animals are particularly useful "models" for improving our understanding of these understudied cancers. Moreover, given several reports that STS subtypes, including UPS, are characterized by aberrant DNA methylation patterns [5–11, 13], careful examination of the underlying mechanisms and functional consequences of this epigenetic modification is critical. Herein, we adopted a comparative oncology approach consisting of human and canine patient-derived cell lines and tissue specimens, together with an orthotopic murine tumor model, to probe the function of DNMTs in UPS and evaluate their potential as anti-neoplastic targets. We found that DNMT3B genetic depletion in UPS cells inhibits proliferation *in vitro* and extends survival *in vivo*, but that an existing DNMT3B-targeting tool compound, nanaomycin A, elicits systemic toxicity, thereby precluding its clinical applicability.

Hypomethylating agents such as DAC and Azacitidine (Vidaza) received FDA approval for the treatment of myelodysplastic syndrome nearly two decades ago. However, innate and acquired resistance to these drugs remains a significant clinical challenge [52–56]. Herein, we showed that innate DAC resistance may also occur in the setting of UPS and revealed a role for hENT1 in this phenomenon. hENT1 (*SLC29A1*) is a member of the SLC29 family of solute transporters, which facilitates the intracellular uptake of nucleosides and nucleoside analogs [57]. hENT1 has been previously implicated in the regulation of DAC response heterogeneity, in that DAC IC_{50} values inversely correlated with *SLC29A1* gene expression levels in a panel of hematologic cancer and carcinoma cell lines [34]. However, whether hENT1 is explicitly required for DAC sensitivity was not explored in this study [34]. Moreover, *SLC29A1* expression levels in bone marrow specimens from myelodysplastic syndrome patients showed no association with responses to DAC therapy [56]. In contrast, we found that hENT1 is both associated with and required for DAC sensitivity in UPS/FS cells. Specifically, genetic depletion of *SLC29A1*, but not the closely

related gene *SLC29A2*, reversed the DAC-induced proliferation deficit observed in HT-1080 FS cells. As *SLC29A1* deficiency strongly impaired HT-1080 cell proliferation at baseline, potentially confounding the experiment, we cannot exclude the possibility that other factors, such as nucleoside metabolizing enzymes, may also regulate DAC sensitivity/resistance. Nevertheless, given our observation that *SLC29A1* expression is highly variable in both human and canine STS specimens, our data suggest that hENT1 plays a critical role in cellular responses to DAC, and illustrate the potential utility of this transporter as a biomarker of DAC response in sarcoma patients.

Given the response heterogeneity of UPS cells/tissues to DAC, we assessed the anti-neoplastic efficacy of a potential alternative, nanaomycin A. To our knowledge, this work is the first to evaluate the therapeutic potential of nanaomycin A in any sarcoma subtype. Consistent with other studies in neuroblastoma, melanoma, leukemia, and colon and lung carcinoma cell lines [43, 58, 59], we found that clinically relevant, nanomolar doses of nanaomycin A potently inhibited UPS cell proliferation without inducing substantial cytotoxicity. However, its efficacy *in vivo* was extremely limited: although the highest evaluated dose almost completely ceased tumor growth in 2/10 animals, these same individuals experienced severe cachexia and were humanely euthanized. Body weights of the remaining mice in this group were also significantly lower than those of control mice. Notably, we are only aware of one other publication that evaluated the anti-neoplastic properties of nanaomycin A *in vivo*, but data pertaining to tumor growth, animal survival and systemic toxicity were not reported [60]. Using computational molecular docking methods and biochemical assays, Kuck and colleagues [43, 61] previously demonstrated that nanaomycin A binds to the active site of DNMT3B, but not DNMT1. However, whether or not the compound also inhibits DNMT3A, which exhibits greater sequence homology to DNMT3B than does DNMT1, was not evaluated [43, 61]. Thus, we hypothesize that dual inhibition of DNMT3A and DNMT3B may at least partially underlie the observed systemic toxicity of nanaomycin A, particularly in light of reports that these paralogs can exhibit functional redundancy in some cell types [62–64]. Nevertheless, given the potency of nanaomycin A *in vitro*, we posit that the development of novel pharmacologic DNMT3B-targeting strategies for UPS, and potentially other DNMT3B-overexpressing/amplified cancers, represents a promising avenue for future research.

Mechanistically, we found that genetic DNMT3B depletion blocks UPS cell proliferation by inhibiting DNA synthesis and causing cells to accumulate in G1-phase of the cell cycle. Similar findings have been reported in rhabdomyosarcoma, a pediatric skeletal muscle tumor [65], as well as in epithelial cancers such as pancreatic and bladder cancers, and cholangiocarcinomas [66–68]. In normal cells, G1-phase growth arrest is typically induced by p53 stabilization and transcription of its downstream targets [69]. However, our work suggests that the growth arrest observed in DNMT3B-deficient UPS cells may be p53-independent, as KP230 cells in particular, like many human UPS tumors, are p53-null. In malignant contexts, p53-independent G1-phase growth arrest can occur via mechanisms such as suppression of c-Myc or downregulation of protein kinase C α and θ [70, 71]. Thus, evaluation of potential crosstalk between DNMT3B and these cell cycle regulators may provide further insight into the molecular susceptibilities of p53-deficient UPS cells.

Several challenges must be overcome before canine companion animals can be widely used as translational and clinical models of STS. First, functional studies in canine cells are currently limited by a paucity of cell lines and reagents (e.g., shRNAs, antibodies). Indeed, in the present study, we were unable to achieve consistent shRNA-mediated knockdown of canine *DNMT3B*, nor were we able to find any suitable shRNA constructs for depletion of *DNMT3A*. Of the experiments in which canine sarcoma cells were used, only one relevant cell line, STSA-1, was available. Thus, widespread commercialization of rigorously validated canine-specific reagents will facilitate broader incorporation of canine models into functional oncology and drug discovery research. In addition, as in the present study, detailed classification of canine STS is not routinely performed in veterinary medicine, largely due to poorly characterized associations among tumor subtype, patient prognosis and therapeutic response [21, 72]. When detailed subtyping is performed, differences in nomenclature and classification conventions often lead to diagnostic inconsistencies between human and veterinary pathologists, even when cross-species tumor histologies are similar [24, 72]. Therefore, development of a more reproducible STS classification system is paramount. Nevertheless, despite these challenges, our study underscores the promise of comparative oncology approaches. Our findings revealed strong parallels between human and canine cells/tissue with respect to multiple aspects of STS biology, including drug sensitivity/resistance patterns, as well as differences in gene expression between tumors and normal skeletal muscle. Ultimately, continued development of translational canine models in this area will provide valuable insight into the biology and treatment of this aggressive disease in both human and canine patients.

Supplementary Material

Refer to Web version on PubMed Central for supplementary material.

Acknowledgements

Availability of data and materials

RNA-seq data from this publication have been deposited into the NCBI Gene Expression Omnibus (GEO) under accession number GSE200026. All other data and materials are available from the corresponding author upon reasonable request.

LIST OF ABBREVIATIONS

DAC	5-aza-2'-deoxycytidine
DNMT	DNA methyltransferase
ER	Epitope retrieval
FDR	False-discovery rate
FS	Fibrosarcoma
H&E	hematoxylin and eosin
IHC	Immunohistochemistry
MFS	Myxofibrosarcoma
ROI	Region of interest
STS	Soft-tissue sarcoma
TCGA-SARC	The Cancer Genome Atlas Sarcoma dataset
TMA	Tissue microarray
UPS	Undifferentiated pleomorphic sarcoma

References

1. Katz D, Palmerini E and Pollack SM, More Than 50 Subtypes of Soft Tissue Sarcoma: Paving the Path for Histology-Driven Treatments. Am Soc Clin Oncol Educ Book. 38, 925–938 (2018) [PubMed: 30231352]

2. Dufresne A, Brahmi M, Karanian M and Blay JY, Using biology to guide the treatment of sarcomas and aggressive connective-tissue tumours. Nat Rev Clin Oncol. 15, 443–458 (2018) [PubMed: 29666441]

3. Fletcher CDM, World Health Organization. and International Agency for Research on Cancer., WHO classification of tumours of soft tissue and bone, 4th edn. (IARC Press, Lyon, 2013).

4. Widemann BC and Italiano A, Biology and Management of Undifferentiated Pleomorphic Sarcoma, Myxofibrosarcoma, and Malignant Peripheral Nerve Sheath Tumors: State of the Art and Perspectives. J Clin Oncol. 36, 160–167 (2018) [PubMed: 29220302]

5. Seidel C, Schagdarsurengin U, Blumke K, Wurl P, Pfeifer GP, Hauptmann S, Taubert H and Dammann R, Frequent hypermethylation of MST1 and MST2 in soft tissue sarcoma. Mol Carcinog. 46, 865–871 (2007) [PubMed: 17538946]

6. Renner M, Wolf T, Meyer H, Hartmann W, Penzel R, Ulrich A, Lehner B, Hovestadt V, Czwan E, Egerer G, Schmitt T, Alldinger I, Renker EK, Ehemann V, Eils R, Wardelmann E, Buttner R, Lichter P, Brors B, Schirmacher P and Mechtersheimer G, Integrative DNA methylation and gene expression analysis in high-grade soft tissue sarcomas. Genome Biol. 14, r137 (2013) [PubMed: 24345474]

7. Merritt NM, Fullenkamp CA, Hall SL, Qian Q, Desai C, Thomason J, Lambertz AM, Dupuy AJ, Darbro B and Tanas MR, A comprehensive evaluation of Hippo pathway silencing in sarcomas. Oncotarget. 9, 31620–31636 (2018) [PubMed: 30167083]

8. Seidel C, Bartel F, Rastetter M, Bluemke K, Wurl P, Taubert H and Dammann R, Alterations of cancer-related genes in soft tissue sarcomas: hypermethylation of RASSF1A is frequently detected

in leiomyosarcoma and associated with poor prognosis in sarcoma. Int J Cancer. 114, 442–447 (2005) [PubMed: 15551306]

9. Kawaguchi K, Oda Y, Saito T, Yamamoto H, Takahira T, Kobayashi C, Tamiya S, Tateishi N, Iwamoto Y and Tsuneyoshi M, DNA hypermethylation status of multiple genes in soft tissue sarcomas. Mod Pathol. 19, 106–114 (2006) [PubMed: 16258501]

10. e.d.s.c. Cancer Genome Atlas Research Network. Electronic address and N. Cancer Genome Atlas Research, Comprehensive and Integrated Genomic Characterization of Adult Soft Tissue Sarcomas. Cell. 171, 950–965 e928 (2017) [PubMed: 29100075]

11. Steele CD, Tarabichi M, Oukrif D, Webster AP, Ye H, Fittall M, Lombard P, Martincorena I, Tarpey PS, Collord G, Haase K, Strauss SJ, Berisha F, Vaikkinen H, Dhami P, Jansen M, Behjati S, Amary MF, Tirabosco R, Feber A, Campbell PJ, Alexandrov LB, Van Loo P, Flanagan AM and Pillay N, Undifferentiated Sarcomas Develop through Distinct Evolutionary Pathways. Cancer Cell. 35, 441–456 e448 (2019) [PubMed: 30889380]

12. Herman JG and Baylin SB, Gene silencing in cancer in association with promoter hypermethylation. N Engl J Med. 349, 2042–2054 (2003) [PubMed: 14627790]

13. Koelsche C, Schrimpf D, Stichel D, Sill M, Sahm F, Reuss DE, Blattner M, Worst B, Heilig CE, Beck K, Horak P, Kreutzfeldt S, Paff E, Stark S, Johann P, Selt F, Ecker J, Sturm D, Pajtler KW, Reinhardt A, Wefers AK, Sievers P, Ebrahimi A, Suwala A, Fernandez-Klett F, Casalini B, Korshunov A, Hovestadt V, Kommoss FKF, Kriegsmann M, Schick M, Bewerunge-Hudler M, Milde T, Witt O, Kulozik AE, Kool M, Romero-Perez L, Grunewald TGP, Kirchner T, Wick W, Platten M, Unterberg A, Uhl M, Abdollahi A, Debus J, Lehner B, Thomas C, Hasselblatt M, Paulus W, Hartmann C, Staszewski O, Prinz M, Hench J, Frank S, Versleijen-Jonkers YMH, Weidema ME, Mentzel T, Griewank K, de Alava E, Martin JD, Gastearena MAI, Chang KT, Low SYY, Cuevas-Bourdier A, Mittelbronn M, Mynarek M, Rutkowski S, Schuller U, Mautner VF, Schittenhelm J, Serrano J, Snuderl M, Buttner R, Klingebiel T, Buslei R, Gessler M, Wesseling P, Dinjens WNM, Brandner S, Jaunmuktane Z, Lyskjaer I, Schirmacher P, Stenzinger A, Brors B, Glimm H, Heining C, Tirado OM, Sainz-Jaspeado M, Mora J, Alonso J, Del Muro XG, Moran S, Esteller M, Benhamida JK, Ladanyi M, Wardelmann E, Antonescu C, Flanagan A, Dirksen U, Hohenberger P, Baumhoer D, Hartmann W, Vokuhl C, Flucke U, Petersen I, Mechtersheimer G, Capper D, Jones DTW, Frohling S, Pfister SM and von Deimling A, Sarcoma classification by DNA methylation profiling. Nat Commun. 12, 498 (2021) [PubMed: 33479225]

14. Yang X, Han H, De Carvalho DD, Lay FD, Jones PA and Liang G, Gene body methylation can alter gene expression and is a therapeutic target in cancer. Cancer Cell. 26, 577–590 (2014) [PubMed: 25263941]

15. Arechederra M, Daian F, Yim A, Bazai SK, Richelme S, Dono R, Saurin AJ, Habermann BH and Maina F, Hypermethylation of gene body CpG islands predicts high dosage of functional oncogenes in liver cancer. Nat Commun. 9, 3164 (2018) [PubMed: 30089774]

16. Lyko F, The DNA methyltransferase family: a versatile toolkit for epigenetic regulation. Nat Rev Genet. 19, 81–92 (2018) [PubMed: 29033456]

17. Paoloni MC and Khanna C, Comparative oncology today. Vet Clin North Am Small Anim Pract. 37, 1023–1032; v (2007) [PubMed: 17950880]

18. Gordon I, Paoloni M, Mazcko C and Khanna C, The Comparative Oncology Trials Consortium: using spontaneously occurring cancers in dogs to inform the cancer drug development pathway. PLoS Med. 6, e1000161 (2009) [PubMed: 19823573]

19. Dennis MM, McSporran KD, Bacon NJ, Schulman FY, Foster RA and Powers BE, Prognostic factors for cutaneous and subcutaneous soft tissue sarcomas in dogs. Vet Pathol. 48, 73–84 (2011) [PubMed: 21139143]

20. Rao SR, Somarelli JA, Altunel E, Selmic LE, Byrum M, Sheth MU, Cheng S, Ware KE, Kim SY, Prinz JA, Devos N, Corcoran DL, Moseley A, Soderblom E, Hsu SD and Eward WC, From the Clinic to the Bench and Back Again in One Dog Year: How a Cross-Species Pipeline to Identify New Treatments for Sarcoma Illuminates the Path Forward in Precision Medicine. Front Oncol. 10, 117 (2020) [PubMed: 32117764]

21. Boerkamp KM, Hellmen E, Willen H, Grinwis GC, Teske E and Rutteman GR, Unclassified sarcomas: a study to improve classification in a cohort of Golden Retriever dogs. J Vet Diagn Invest. 28, 623–631 (2016) [PubMed: 27698172]

22. Chijiwa K, Uchida K and Tateyama S, Immunohistochemical evaluation of canine peripheral nerve sheath tumors and other soft tissue sarcomas. Vet Pathol. 41, 307–318 (2004) [PubMed: 15232130]

23. Iwaki Y, Lindley S, Smith A, Curran KM and Looper J, Canine myxosarcomas, a retrospective analysis of 32 dogs (2003–2018). BMC Vet Res. 15, 217 (2019) [PubMed: 31248415]

24. Milovancev M, Hauck M, Keller C, Stranahan LW, Mansoor A and Malarkey DE, Comparative pathology of canine soft tissue sarcomas: possible models of human non-rhabdomyosarcoma soft tissue sarcomas. J Comp Pathol. 152, 22–27 (2015) [PubMed: 25435513]

25. Schweiger N, Hauck M, Steinhoff H, Sampl S, Reifinger M, Walter I, Kreilmeier T, Marian B, Grusch M, Berger W, Holzmann K and Kleiter M, Canine and human sarcomas exhibit predominant FGFR1 expression and impaired viability after inhibition of signaling. Mol Carcinog. 54, 841–852 (2015) [PubMed: 24719266]

26. Eisinger-Mathason TS, Zhang M, Qiu Q, Skuli N, Nakazawa MS, Karakasheva T, Mucaj V, Shay JE, Stangenberg L, Sadri N, Pure E, Yoon SS, Kirsch DG and Simon MC, Hypoxia-dependent modification of collagen networks promotes sarcoma metastasis. Cancer Discov. 3, 1190–1205 (2013) [PubMed: 23906982]

27. Love MI, Huber W and Anders S, Moderated estimation of fold change and dispersion for RNA-seq data with DESeq2. Genome Biol. 15, 550 (2014) [PubMed: 25516281]

28. Patro R, Duggal G, Love MI, Irizarry RA and Kingsford C, Salmon provides fast and bias-aware quantification of transcript expression. Nat Methods. 14, 417–419 (2017) [PubMed: 28263959]

29. Zhou Y, Zhou B, Pache L, Chang M, Khodabakhshi AH, Tanaseichuk O, Benner C and Chanda SK, Metascape provides a biologist-oriented resource for the analysis of systems-level datasets. Nat Commun. 10, 1523 (2019) [PubMed: 30944313]

30. Riccardi C and Nicoletti I, Analysis of apoptosis by propidium iodide staining and flow cytometry. Nat Protoc. 1, 1458–1461 (2006) [PubMed: 17406435]

31. Derissen EJ, Beijnen JH and Schellens JH, Concise drug review: azacitidine and decitabine. Oncologist. 18, 619–624 (2013) [PubMed: 23671007]

32. Saba HI, Decitabine in the treatment of myelodysplastic syndromes. Ther Clin Risk Manag. 3, 807–817 (2007) [PubMed: 18473005]

33. Tsai HC, Li H, Van Neste L, Cai Y, Robert C, Rassool FV, Shin JJ, Harbom KM, Beaty R, Pappou E, Harris J, Yen RW, Ahuja N, Brock MV, Stearns V, Feller-Kopman D, Yarmus LB, Lin YC, Welm AL, Issa JP, Minn I, Matsui W, Jang YY, Sharkis SJ, Baylin SB and Zahnow CA, Transient low doses of DNA-demethylating agents exert durable antitumor effects on hematological and epithelial tumor cells. Cancer Cell. 21, 430–446 (2012) [PubMed: 22439938]

34. Qin T, Jelinek J, Si J, Shu J and Issa JP, Mechanisms of resistance to 5-aza-2'-deoxycytidine in human cancer cell lines. Blood. 113, 659–667 (2009) [PubMed: 18931345]

35. Detwiller KY, Fernando NT, Segal NH, Ryeom SW, D'Amore PA and Yoon SS, Analysis of hypoxia-related gene expression in sarcomas and effect of hypoxia on RNA interference of vascular endothelial cell growth factor A. Cancer Res. 65, 5881–5889 (2005) [PubMed: 15994966]

36. Gentschev I, Adelfinger M, Josupeit R, Rudolph S, Ehrig K, Donat U, Weibel S, Chen NG, Yu YA, Zhang Q, Heisig M, Thamm D, Stritzker J, Macneill A and Szalay AA, Preclinical evaluation of oncolytic vaccinia virus for therapy of canine soft tissue sarcoma. PLoS One. 7, e37239 (2012) [PubMed: 22615950]

37. Kirsch DG, Dinulescu DM, Miller JB, Grimm J, Santiago PM, Young NP, Nielsen GP, Quade BJ, Chaber CJ, Schultz CP, Takeuchi O, Bronson RT, Crowley D, Korsmeyer SJ, Yoon SS, Hornicek FJ, Weissleder R and Jacks T, A spatially and temporally restricted mouse model of soft tissue sarcoma. Nat Med. 13, 992–997 (2007) [PubMed: 17676052]

38. Mito JK, Riedel RF, Dodd L, Lahat G, Lazar AJ, Dodd RD, Stangenberg L, Eward WC, Hornicek FJ, Yoon SS, Brigman BE, Jacks T, Lev D, Mukherjee S and Kirsch DG, Cross species genomic analysis identifies a mouse model as undifferentiated pleomorphic sarcoma/malignant fibrous histiocytoma. PLoS One. 4, e8075 (2009) [PubMed: 19956606]

39. Mizushima N, Yoshimori T and Levine B, Methods in mammalian autophagy research. Cell. 140, 313–326 (2010) [PubMed: 20144757]

40. Yoshii SR and Mizushima N, Monitoring and Measuring Autophagy. Int J Mol Sci. 18, (2017)

41. Srinivas V, Kitagawa M, Wong J, Liao PJ and Lee SH, The Tumor Suppressor Cdkn3 Is Required for Maintaining the Proper Number of Centrosomes by Regulating the Centrosomal Stability of Mps1. Cell Rep. 13, 1569–1577 (2015) [PubMed: 26586430]

42. Masamha CP and Benbrook DM, Cyclin D1 degradation is sufficient to induce G1 cell cycle arrest despite constitutive expression of cyclin E2 in ovarian cancer cells. Cancer Res. 69, 6565–6572 (2009) [PubMed: 19638577]

43. Kuck D, Caulfield T, Lyko F and Medina-Franco JL, Nanaomycin A selectively inhibits DNMT3B and reactivates silenced tumor suppressor genes in human cancer cells. Mol Cancer Ther. 9, 3015–3023 (2010) [PubMed: 20833755]

44. Omura S, Tanaka H, Koyama Y, Oiwa R and Katagiri M, Letter: Nanaomycins A and B, new antibiotics produced by a strain of Streptomyces. J Antibiot (Tokyo). 27, 363–365 (1974) [PubMed: 4852870]

45. Wong CC, Cheng KW and Rigas B, Preclinical predictors of anticancer drug efficacy: critical assessment with emphasis on whether nanomolar potency should be required of candidate agents. J Pharmacol Exp Ther. 341, 572–578 (2012) [PubMed: 22448039]

46. La Rovere RM, Quattrocelli M, Pietrangelo T, Di Filippo ES, Maccatrozzo L, Cassano M, Mascarello F, Barthelemy I, Blot S, Sampaolesi M and Fulle S, Myogenic potential of canine craniofacial satellite cells. Front Aging Neurosci. 6, 90 (2014) [PubMed: 24860499]

47. Owens J, Moreira K and Bain G, Characterization of primary human skeletal muscle cells from multiple commercial sources. In Vitro Cell Dev Biol Anim. 49, 695–705 (2013) [PubMed: 23860742]

48. Rivera-Reyes A, Ye S, G EM, Egolf S, G EC,Chor S, Liu Y, Posimo JM, Park PMC, Pak K, Babichev Y, Sostre-Colon J, Tameire F, Leli NM, Koumenis C, D CB, Mancuso A, Weber K, Gladdy R, Qi Jand Eisinger-Mathason TSK, YAP1 enhances NF-kappaB-dependent and independent effects on clock-mediated unfolded protein responses and autophagy in sarcoma. Cell Death Dis. 9, 1108 (2018) [PubMed: 30382078]

49. Smerdu V, Strbenc M, Meznaric-Petrusa M and Fazarinc G, Identification of myosin heavy chain I, IIa and IIx in canine skeletal muscles by an electrophoretic and immunoblotting study. Cells Tissues Organs. 180, 106–116 (2005) [PubMed: 16113539]

50. Strbenc M, Smerdu V, Pogacnik A and Fazarinc G, Myosin heavy chain isoform transitions in canine skeletal muscles during postnatal growth. J Anat. 209, 149–163 (2006) [PubMed: 16879596]

51. Schober P, Boer C and Schwarte LA, Correlation Coefficients: Appropriate Use and Interpretation. Anesth Analg. 126, 1763–1768 (2018) [PubMed: 29481436]

52. Fenaux P, Mufti GJ, Hellstrom-Lindberg E, Santini V, Finelli C, Giagounidis A, Schoch R, Gattermann N, Sanz G, List A, Gore SD, Seymour JF, Bennett JM, Byrd J, Backstrom J, Zimmerman L, McKenzie D, Beach C, Silverman LR and M.D.S.S.S.G. International Vidaza High-Risk, Efficacy of azacitidine compared with that of conventional care regimens in the treatment of higher-risk myelodysplastic syndromes: a randomised, open-label, phase III study. Lancet Oncol. 10, 223–232 (2009) [PubMed: 19230772]

53. Jabbour E, Garcia-Manero G, Batty N, Shan J, O'Brien S, Cortes J, Ravandi F, Issa JP and Kantarjian H, Outcome of patients with myelodysplastic syndrome after failure of decitabine therapy. Cancer. 116, 3830–3834 (2010) [PubMed: 20564137]

54. Prebet T, Gore SD, Esterni B, Gardin C, Itzykson R, Thepot S, Dreyfus F, Rauzy OB, Recher C, Ades L, Quesnel B, Beach CL, Fenaux P and Vey N, Outcome of high-risk myelodysplastic syndrome after azacitidine treatment failure. J Clin Oncol. 29, 3322–3327 (2011) [PubMed: 21788559]

55. Prebet T, Gore SD, Thepot S, Esterni B, Quesnel B, Beyne Rauzy O, Dreyfus F, Gardin C, Fenaux P and Vey N, Outcome of acute myeloid leukaemia following myelodysplastic syndrome after azacitidine treatment failure. Br J Haematol. 157, 764–766 (2012) [PubMed: 22390719]

56. Qin T, Castoro R, El Ahdab S, Jelinek J, Wang X, Si J, Shu J, He R, Zhang N, Chung W, Kantarjian HM and Issa JP, Mechanisms of resistance to decitabine in the myelodysplastic syndrome. PLoS One. 6, e23372 (2011) [PubMed: 21858090]

57. Young JD, The SLC28 (CNT) and SLC29 (ENT) nucleoside transporter families: a 30-year collaborative odyssey. Biochem Soc Trans. 44, 869–876 (2016) [PubMed: 27284054]

58. Penter L, Maier B, Frede U, Hackner B, Carell T, Hagemeier C and Truss M, A rapid screening system evaluates novel inhibitors of DNA methylation and suggests F-box proteins as potential therapeutic targets for high-risk neuroblastoma. Target Oncol. 10, 523–533 (2015) [PubMed: 25559288]

59. Sztiller-Sikorska M, Koprowska K, Majchrzak K, Hartman M and Czyz M, Natural compounds' activity against cancer stem-like or fast-cycling melanoma cells. PLoS One. 9, e90783 (2014) [PubMed: 24595456]

60. Lai SC, Su YT, Chi CC, Kuo YC, Lee KF, Wu YC, Lan PC, Yang MH, Chang TS and Huang YH, DNMT3b/OCT4 expression confers sorafenib resistance and poor prognosis of hepatocellular carcinoma through IL-6/STAT3 regulation. J Exp Clin Cancer Res. 38, 474 (2019) [PubMed: 31771617]

61. Kuck D, Singh N, Lyko F and Medina-Franco JL, Novel and selective DNA methyltransferase inhibitors: Docking-based virtual screening and experimental evaluation. Bioorg Med Chem. 18, 822–829 (2010) [PubMed: 20006515]

62. Challen GA, Sun D, Mayle A, Jeong M, Luo M, Rodriguez B, Mallaney C, Celik H, Yang L, Xia Z, Cullen S, Berg J, Zheng Y, Darlington GJ, Li W and Goodell MA, Dnmt3a and Dnmt3b have overlapping and distinct functions in hematopoietic stem cells. Cell Stem Cell. 15, 350–364 (2014) [PubMed: 25130491]

63. D'Antonio M, Pendino V, Sinha S and Ciccarelli FD, Network of Cancer Genes (NCG 3.0): integration and analysis of genetic and network properties of cancer genes. Nucleic Acids Res. 40, D978–983 (2012) [PubMed: 22080562]

64. Liao J, Karnik R, Gu H, Ziller MJ, Clement K, Tsankov AM, Akopian V, Gifford CA, Donaghey J, Galonska C, Pop R, Reyon D, Tsai SQ, Mallard W, Joung JK, Rinn JL, Gnirke A and Meissner A, Targeted disruption of DNMT1, DNMT3A and DNMT3B in human embryonic stem cells. Nat Genet. 47, 469–478 (2015) [PubMed: 25822089]

65. Megiorni F, Camero S, Ceccarelli S, McDowell HP, Mannarino O, Marampon F, Pizer B, Shukla R, Pizzuti A, Marchese C, Clerico A and Dominici C, DNMT3B in vitro knocking-down is able to reverse embryonal rhabdomyosarcoma cell phenotype through inhibition of proliferation and induction of myogenic differentiation. Oncotarget. 7, 79342–79356 (2016) [PubMed: 27764816]

66. Ying Y, Li J, Xie H, Yan H, Jin K, He L, Ma X, Wu J, Xu X, Fang J, Wang X, Zheng X, Liu B and Xie L, CCND1, NOP14 and DNMT3B are involved in miR-502–5p-mediated inhibition of cell migration and proliferation in bladder cancer. Cell Prolif. 53, e12751 (2020) [PubMed: 31971654]

67. Cao K, Li B, Zhang YW, Song H, Chen YG, Gong YJ, Li HY and Zuo S, miR-29b restrains cholangiocarcinoma progression by relieving DNMT3B-mediated repression of CDKN2B expression. Aging (Albany NY). 13, 6055–6065 (2021) [PubMed: 33601338]

68. Gao J, Wang L, Xu J, Zheng J, Man X, Wu H, Jin J, Wang K, Xiao H, Li S and Li Z, Aberrant DNA methyltransferase expression in pancreatic ductal adenocarcinoma development and progression. J Exp Clin Cancer Res. 32, 86 (2013) [PubMed: 24423239]

69. Agarwal ML, Agarwal A, Taylor WR and Stark GR, p53 controls both the G2/M and the G1 cell cycle checkpoints and mediates reversible growth arrest in human fibroblasts. Proc Natl Acad Sci U S A. 92, 8493–8497 (1995) [PubMed: 7667317]

70. Deeds L, Teodorescu S, Chu M, Yu Q and Chen CY, A p53-independent G1 cell cycle checkpoint induced by the suppression of protein kinase C alpha and theta isoforms. J Biol Chem. 278, 39782–39793 (2003) [PubMed: 12896972]

71. Jeong JH, Kang SS, Park KK, Chang HW, Magae J and Chang YC, p53-independent induction of G1 arrest and p21WAF1/CIP1 expression by ascofuranone, an isoprenoid antibiotic, through downregulation of c-Myc. Mol Cancer Ther. 9, 2102–2113 (2010) [PubMed: 20587660]

72. Seguin B, Canine Soft Tissue Sarcomas: Can Being a Dog's Best Friend Help a Child? Front Oncol. 7, 285 (2017) [PubMed: 29218302]
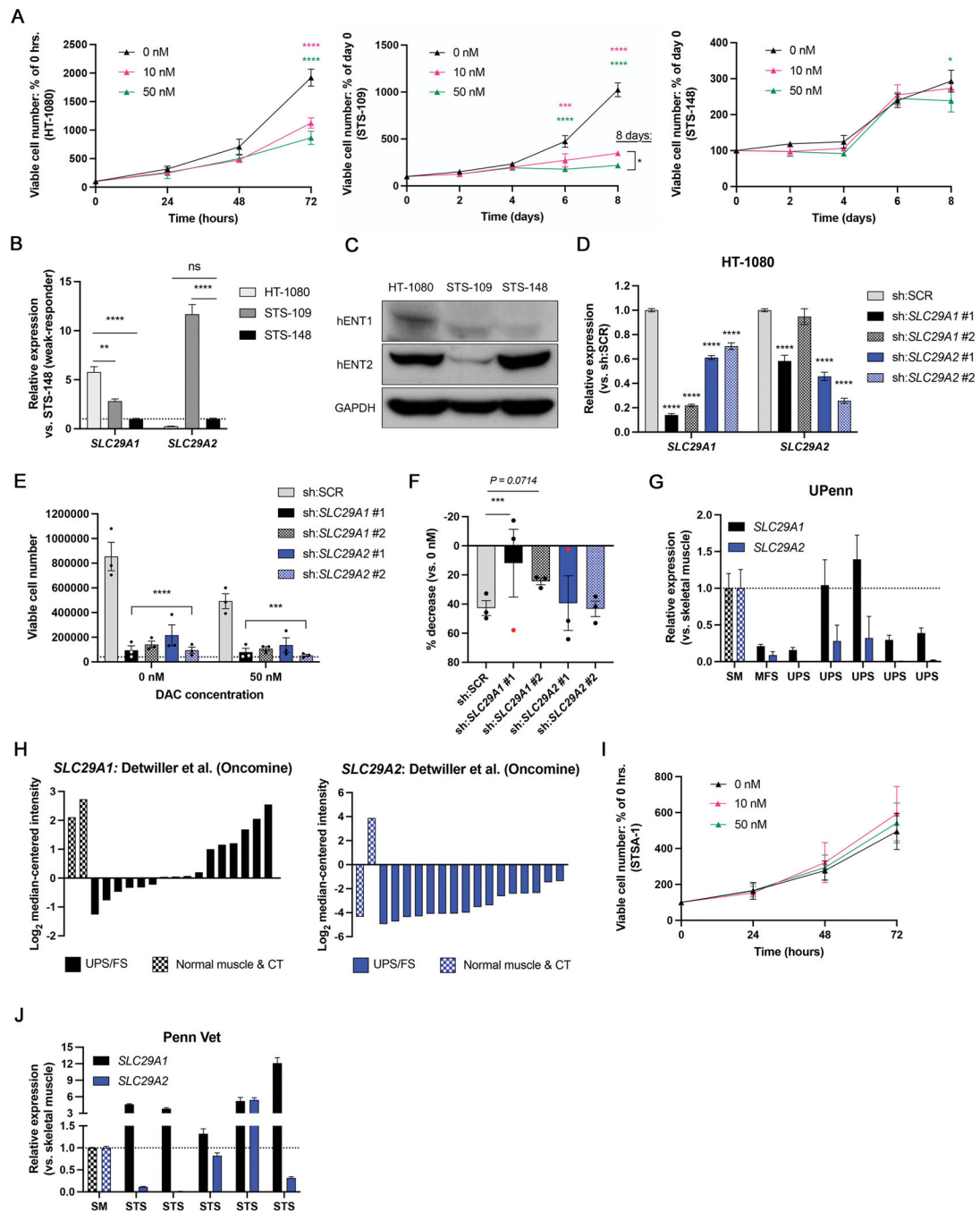
Fig. 1. Response heterogeneity of UPS to 5-aza-2'-deoxycytidine (DAC): role of *SLC29A1*/hENT1.
a. Growth curves of human UPS and FS cells treated daily with clinically relevant,
nanomolar doses of DAC. Two-way ANOVA with Tukey's. Colored asterisks at each
time point indicate significance relative to DMSO. Mean ± SEM. n = 3. **b.** Expression of
nucleoside transporter genes in human UPS/FS cell lines. One-way ANOVA with Dunnett's.
Mean ± SEM. n = 3. **c.** Representative Western blot showing hENT1 and hENT2 protein
expression in human UPS/FS cell lines (n = 3). **d.** Levels of *SLC29A1* and *SLC29A2* gene
expression in human HT-1080 cells from **e** and **f** expressing a scrambled control (sh:SCR),

SLC29A1-, or *SLC29A2*-targeting shRNA lentivirus. **e.** Number of viable HT-1080 cells from **d** and **f** following treatment with 50 nM DAC or DMSO control. Dotted line at 40,000 indicates the number of viable cells seeded prior to drug treatment. Two-way ANOVA with Dunnett's; for each dose, significance is relative to sh:SCR. Mean ± SEM. n = 3. **f.** Percent decrease in the number of HT-1080 cells from **d** and **e** following treatment with 50 nM DAC. Positive values represent a percent decrease; negative values represent a percent increase. One-way ANOVA with Dunnett's (vs. sh:SCR); red points are outliers excluded from the statistical analysis. Mean ± SEM; n = 3. **g.** *SLC29A1* and *SLC29A2* gene expression in human UPS and MFS tumors relative to normal skeletal muscle (SM) tissue (UPenn cohort). Two cDNA samples per specimen. Mean ± SD. **h.** *SLC29A1* and *SLC29A2* gene expression in UPS and FS tissue specimens from the Detwiller et al. sarcoma dataset (Oncomine). CT = connective tissue. **i.** Growth curves of canine STSA-1 cells treated daily with DAC. Two-way ANOVA with Tukey's. Not significant. Mean ± SEM. n =3. **j.** *SLC29A1* and *SLC29A2* gene expression in canine STS samples relative to normal skeletal muscle (SM) tissue (Penn Vet cohort). Mean ± SD. For all panels, $*p < 0.05$, $**p < 0.01$, $***p < 0.001$, $****p < 0.0001$.
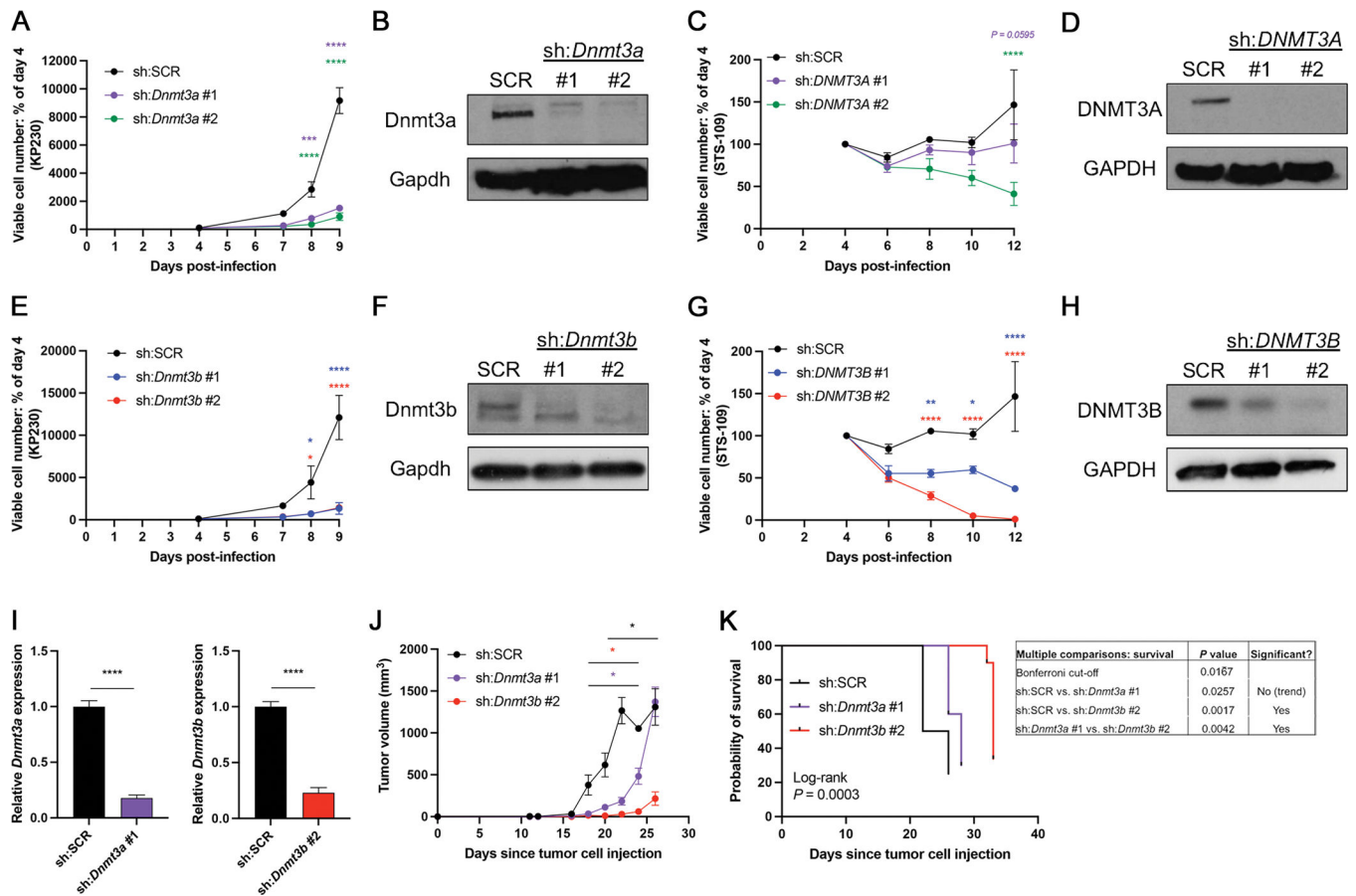
Fig. 2. *DNMT3A* or *DNMT3B* depletion inhibits UPS cell proliferation *in vitro* and *in vivo*. **a.** Growth curves of sh:SCR and sh:*Dnmt3a*-expressing KP230 cells. Two-way ANOVA with Dunnett's (vs. sh:SCR). Mean ± SEM. n = 3. **b.** Representative Western blot of cells in **a**. Brightness enhanced for presentation. **c.** Growth curves of sh:SCR and sh:*DNMT3A*-expressing STS-109 cells. Two-way ANOVA with Dunnett's (vs. sh:SCR). Mean ± SEM. n = 3. **d.** Representative Western blot of cells in **c**. Brightness enhanced for presentation. **e.** Growth curves of sh:SCR and sh:*Dnmt3b*-expressing KP230 cells. Two-way ANOVA with Dunnett's (vs. sh:SCR). Mean ± SEM. n = 3. **f.** Representative Western blot of cells in **e**. Brightness and contrast enhanced for presentation. Top Dnmt3b band in each lane represents the canonical isoform (isoform 1). **g.** Growth curves of sh:SCR and sh:*DNMT3B*-expressing STS-109 cells. Two-way ANOVA with Dunnett's (vs. sh:SCR). Mean ± SEM. n = 3. **h.** Representative Western blot of cells in **g**. Brightness and contrast enhanced for presentation. **i.** *Dnmt3a* and *Dnmt3b* gene expression in KP230 cells orthotopically injected into the gastrocnemius muscles of nude mice. Two-tailed unpaired t-tests. Mean ± SD. **j.** Orthotopic KP230 tumor progression curves. Curves in this panel were terminated when the final mouse in the control group (sh:SCR) was euthanized; full curves are presented in Supplementary Fig. 1o. The "dip" in the sh:SCR curve (day 24) occurred because only 1 mouse remained at this time point. Mixed model with Tukey's. Colored asterisks indicate significance relative to sh:SCR. Black asterisk indicates significance of sh:*Dnmt3b* vs. sh:*Dnmt3a*. Mean ± SEM. n = 10 tumors (5 mice) per group; 1 sh:*Dnmt3b* tumor did not form. **k.** Survival

of orthotopic KP230 tumor-bearing mice from **j**. Log-rank test with Bonferroni correction (table). For all panels, $*p < 0.05$, $**p < 0.01$, $***p < 0.001$, $****p < 0.0001$.
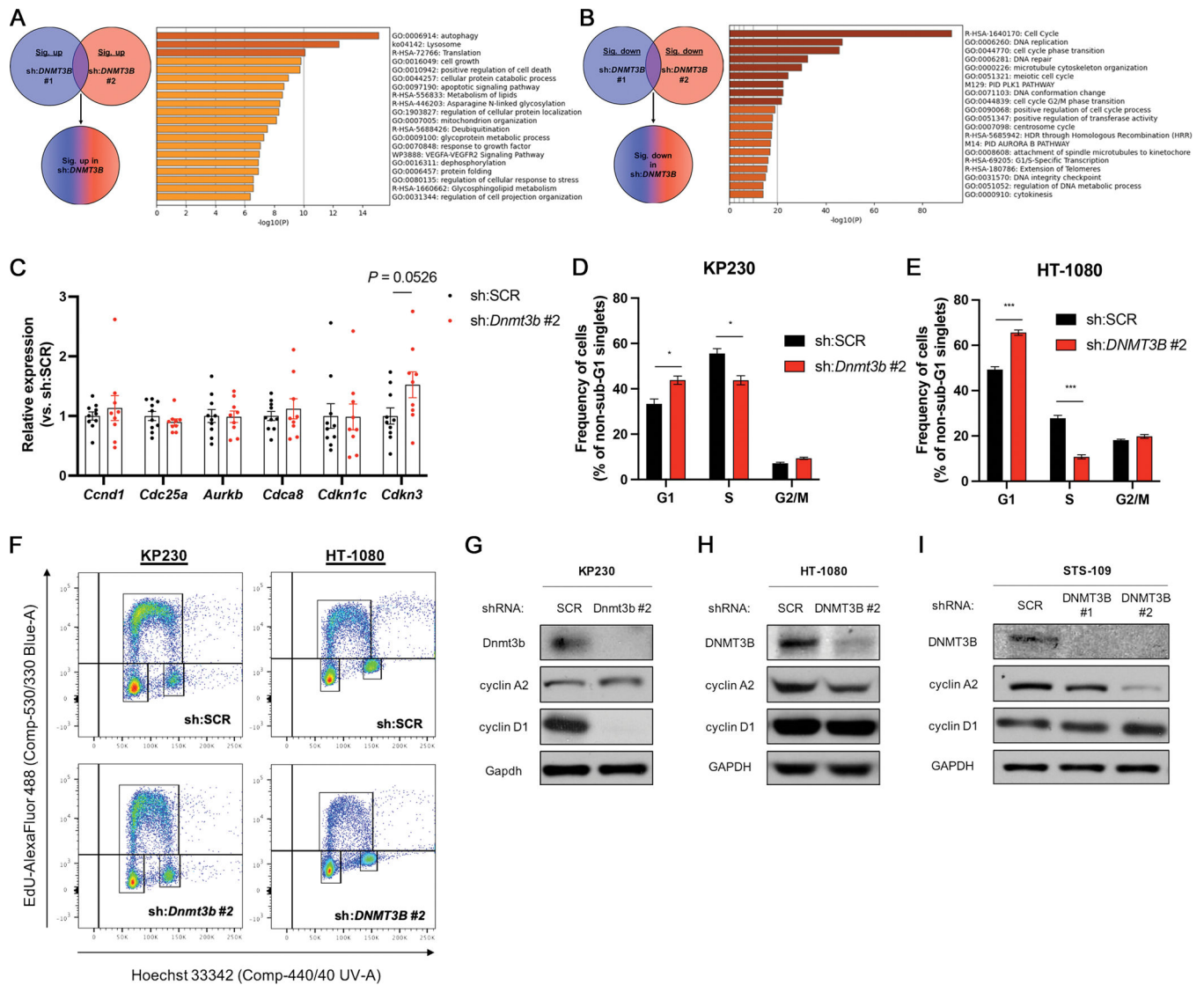
Fig. 3. DNMT3B depletion in UPS cells inhibits DNA synthesis.
a. Schematic and Metascape pathway analysis of genes significantly upregulated in
sh:*DNMT3B*-expressing vs. sh:SCR human STS-109 cells (FDR $p < 0.05$). n = 4.
b. Schematic and Metascape pathway analysis of genes significantly downregulated in
sh:*DNMT3B*-expressing vs. sh:SCR human STS-109 cells (FDR $p < 0.05$). n = 4. **c.**
Expression of cell cycle-related genes in murine KP230 orthotopic bulk tumor specimens.
Two-tailed unpaired t-tests. Mean ± SEM. n = 10 tumors (5 mice) per group; 1 sh:*Dnmt3b*
tumor did not form. **d**. Cell cycle phase frequency distributions of KP230 cells expressing
control or *Dnmt3b*-targeting shRNAs. Two-tailed unpaired t-tests. Mean ± SEM. n = 3. **e.**
Cell cycle phase frequency distributions of HT-1080 cells expressing control or *DNMT3B*-
targeting shRNAs. Two-tailed unpaired t-tests. Mean ± SEM. n = 3. **f.** Representative flow
cytometry plots from **d-e**. **g-i.** Representative Western blots of cyclin D1 and cyclin A2
expression in control and *Dnmt3b/DNMT3B*-deficient KP230 (n = 3), HT-1080 (n = 3), and

STS-109 (n = 2) cells. Brightness and contrast of Dnmt3b/DNMT3B panels were adjusted for presentation. For all panels, $*p < 0.05$, $***p < 0.001$.
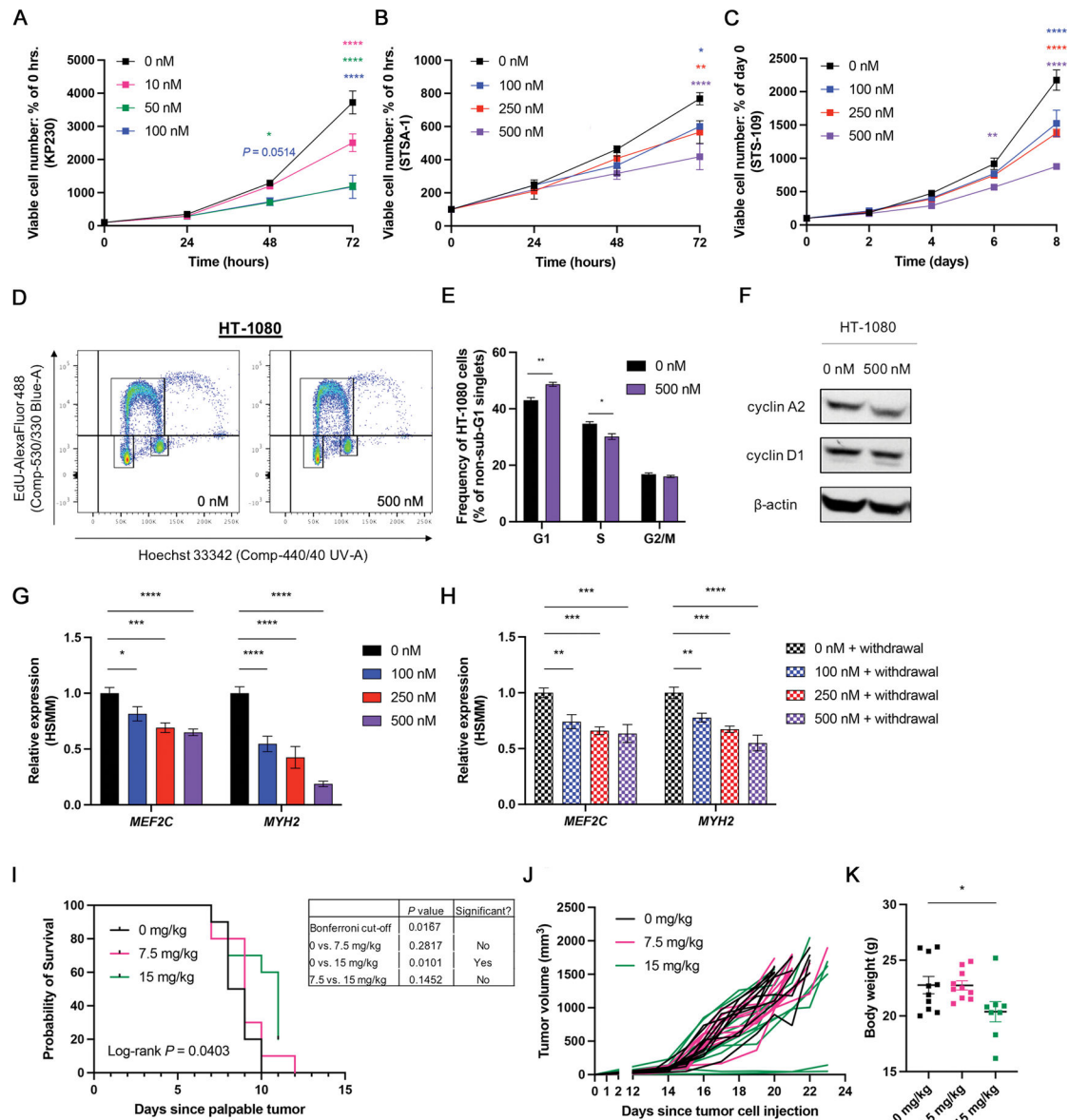
Fig. 4. DNMT3B inhibitor nanaomycin A impedes UPS cell proliferation *in vitro*.
a-c. Growth curves of KP230 (**a**), STSA-1 (**b**) and STS-109 (**c**) cells treated daily with nanaomycin A. Two-way ANOVA with Tukey's. Asterisks represent significance relative to 0 nM. For ease of visualization, only statistical comparisons vs. 0 nM are presented in the figure. Full statistical results for all possible comparisons are shown in Supplementary Table 4. Mean ± SEM. n   3. **d**. Representative flow cytometry plots showing cell cycle phase distributions of control and nanaomycin A-treated HT-1080 cells. **e**. Quantification of HT-1080 cell cycle phase distributions shown in **d**. Two-tailed unpaired t-tests. Mean ±

SEM. n = 3. **f.** Representative Western blot of cyclin D1 and cyclin A2 expression in control and nanaomycin A-treated HT-1080 cells (n = 3). Contrast enhanced for presentation. **g.** Expression of human skeletal muscle lineage markers in HSMM myoblasts exposed to nanaomycin A or vehicle control over the course of differentiation to myotubes. One-way ANOVA with Dunnett's (vs. 0 nM). Mean ± SEM. n = 3. **h.** Expression of human skeletal muscle lineage markers in control- or nanaomycin A-treated HSMM myoblasts 5 days after drug withdrawal. One-way ANOVA with Dunnett's (vs. 0 nM). Mean ± SEM. n = 3. **i.** Survival of orthotopic KP230 tumor-bearing nude mice treated with nanaomycin A or vehicle control. Log-rank test with Bonferroni multiple comparisons correction (table). n = 10 mice per group. **j.** Orthotopic KP230 tumor progression curves of control- and nanaomycin A-treated nude mice shown in **i**. **k.** Body weights of orthotopic KP230 tumor-bearing nude mice from **i-j** immediately prior to euthanasia. Two mice in the 15 mg/kg group that were humanely euthanized prior to the study endpoint are not shown. One-way ANOVA with Dunnett's (vs. 0 mg/kg). Mean ± SEM. For all panels, $*p < 0.05$, $**p < 0.01$, $***p < 0.001$, $****p < 0.0001$.
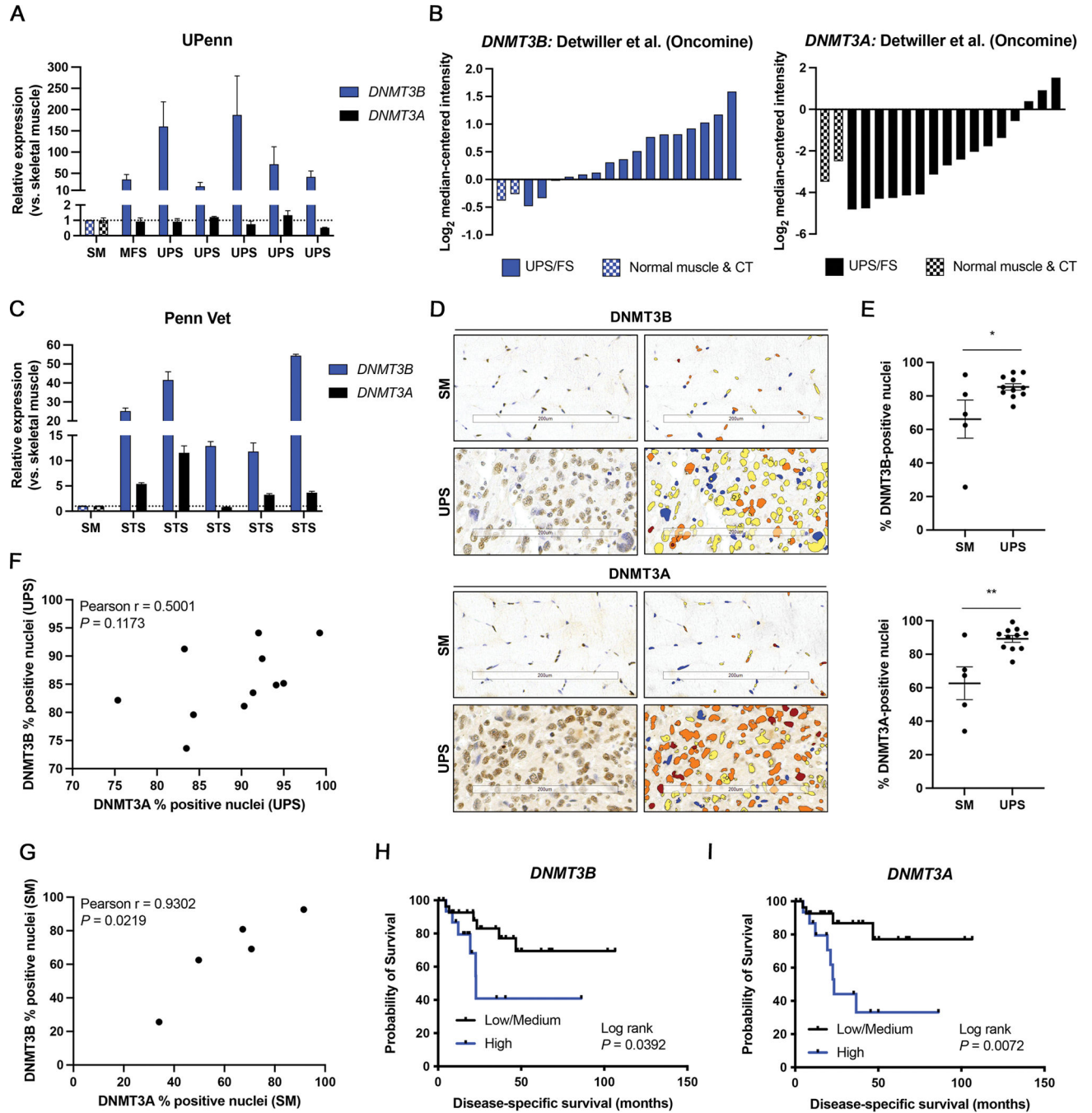
Fig. 5. DNMT3B is overexpressed in human and canine UPS and associated with a poor prognosis.

a. *DNMT3B* and *DNMT3A* gene expression in human UPS and MFS tumors relative to normal skeletal muscle (SM) tissue (UPenn cohort). Two cDNA samples per specimen. Mean ± SD. **b.** *DNMT3B* and *DNMT3A* gene expression in UPS and FS tissue specimens from the Detwiller et al. sarcoma dataset (Oncomine). CT = connective tissue. **c.** *DNMT3B* and *DNMT3A* gene expression in canine STS samples relative to normal skeletal muscle (SM) tissue (Penn Vet cohort). Mean ± SD. **d.** Representative images of DNMT3B and

DNMT3A IHC staining and algorithm-based detection of nuclear immunoreactivity in normal skeletal muscle (SM) and UPS specimens (sarcoma tissue microarray; TMA). Red, orange, yellow, and blue represent 3+, 2+, 1+ and 0+ (negative) staining intensity, respectively. Scale bar = 200 μM. Brightness and contrast have been enhanced for presentation. **e.** Quantification of DNMT3B and DNMT3A percent positive nuclei in normal skeletal muscle (SM) and UPS specimens (sarcoma TMA). Two-tailed unpaired t-test. Mean ± SEM. **f.** Pearson's correlation between the percentage of DNMT3B- and DNMT3A-positive nuclei in UPS specimens from panels d-e. Shapiro-Wilk W value = 0.9553. **g.** Pearson's correlation between the percentage of DNMTB- and DNMT3A-positive nuclei in normal skeletal muscle (SM) specimens from panels **d-e.** Shapiro-Wilk W value = 0.9282. **h-i.** Disease-specific survival of human UPS patients in TCGA Sarcoma (TCGA-SARC) dataset stratified by tumor gene expression levels of *DNMT3B* (**h**) and *DNMT3A* (**i**). Each tertile (low, medium, and high) represents one-third of patients. Log-rank test. n = 44 patients. For all panels, $*p < 0.05$, $**p < 0.01$.